RSC Advances

PAPER

View Article Online
View Journal | View Issue

Cite this: *RSC Adv.*, 2020, **10**, 29475

Design, synthesis and *in silico* studies of new quinazolinone derivatives as antitumor PARP-1 inhibitors†

Sayed K. Ramadan, [a] Eman Z. Elrazaz, [b] Khaled A. M. Abouzid *[bc] and Abeer M. El-Naggar *[a]

Received 7th July 2020
Accepted 27th July 2020

DOI: 10.1039/d0ra05943a

rsc.li/rsc-advances

Herein, we report an eco-friendly synthesis of a new series of quinazolinone-based derivatives as potential PARP-1 inhibitors. The 4-quinazolinone scaffold was utilized as a bioisostere to the phthalazinone core of the reference compound **Olaparib**. Most of the synthesized compounds displayed appreciable inhibitory activity against PARP-1. Compound **12c** showed inhibitory activity at IC_{50} = 30.38 nM comparable to **Olaparib**, which has IC_{50} = 27.89 nM. Cell cycle analysis was performed for compounds **12a** and **12c**, and both exhibited cell growth arrest at G2/M phase in the MCF-7 cell line. In addition, both compounds increased the programmed apoptosis compared to the control. Furthermore, molecular docking of the final compounds into the PARP-1 active site was executed to explore their probable binding modes. Also, a computational QSAR and *in silico* ADMET study was performed. The results of this study revealed that some of the newly synthesized compounds could serve as a new framework to discover new PARP-1 inhibitors with anti-cancer activity.

1. Introduction

Recently, great attention has been given to the PARP-1 enzyme as a promising anti-cancer therapeutic target[1] as it is a member of the PARP family of proteins, which play a crucial role in the repair of single-stranded DNA breaks *via* the base excision repair pathway.[2] In addition, PARP-1 has a major role in a variety of cellular processes, like cellular differentiation, gene transcription, inflammation, mitosis, and cell death, which contribute to the antitumor activity of PARP-1 inhibitors.[3] PARP-1 inhibition has a synthetic lethality in the presence of mutations of BRCA 1/2, which are essential proteins in homologous recombination (HR) of DNA double strand breaks, due to the dependence of the mutant cancer cells on PARP-1 for DNA repair and cell survival.[4,5] Thus, compounds acting as PARP-1 inhibitors may lead to selective cell death, particularly in ovarian and breast cancers.[6] Several PARP-1 inhibitors have already been FDA approved, including AG014699 (**Rucaparib**), AZD2281 (**Olaparib**), MK4827 (**Niraparib**), and BMN673 (**Talazoparib**) (Fig. 1).[7–11]

As a response to DNA damage, PARP-1 catalyzes the cleavage of nicotinamide adenine dinucleotide NAD^+ into nicotinamide and ADP ribose units, which are transferred to different acceptor proteins participating in DNA damage repair processes, including itself, histones and formed ADP-ribose polymers (PAR). So, PARP-1 has two binding sites; one is occupied by the nicotinamide-ribose (NI site) and the other is the adenine-ribose binding site (AD site).[12]

2. Rationale and design

The majority of the reported PARP-1 inhibitors occupy the NI site through hydrogen bonding and pi–pi stacking interactions, and some of them exhibit additional interactions in the AD site, which is large enough to accommodate diverse structures and thus increases their potency, as for **Olaparib**.[13,14] Since the quinazoline nucleus represents a privileged scaffold in many anticancer drugs,[15] in this study, we employed the quinazolinone scaffold as a bioisostere of the phthalazinone core of **Olaparib** to occupy the NI site of PARP-1, since many quinazoline-based compounds are known as anticancer agents.[16] Also, a series of quinazolinone derivatives were synthesized as PARP-1 inhibitors. Among this series, compound **X** displayed the highest inhibitory activity[17,18] (Fig. 1). Therefore, we decided to introduce various substitutions at position-2 of the quinazolinone ring to explore additional interactions with the AD site; the linker aims to mimic the carbonyl group of **Olaparib** and engage with the enzyme through hydrogen bonding and a hydrophobic moiety was added to mimic the cyclopropyl group of **Olaparib**. The newly synthesized compounds were tested for their inhibitory activities against the PARP-1 enzyme (Fig. 1).

[a]*Department of Chemistry, Faculty of Science, Ain Shams University, Abbassia, 11566 Cairo, Egypt. E-mail: elsayedam@sci.asu.edu.eg*

[b]*Department of Pharmaceutical Chemistry, Faculty of Pharmacy, Ain Shams University, Abbassia, 11566 Cairo, Egypt. E-mail: khaled.abouzid@pharma.asu.edu.eg*

[c]*Department of Organic and Medicinal Chemistry, Faculty of Pharmacy, University of Sadat City, Sadat City, Egypt*

† Electronic supplementary information (ESI) available. See DOI: 10.1039/d0ra05943a

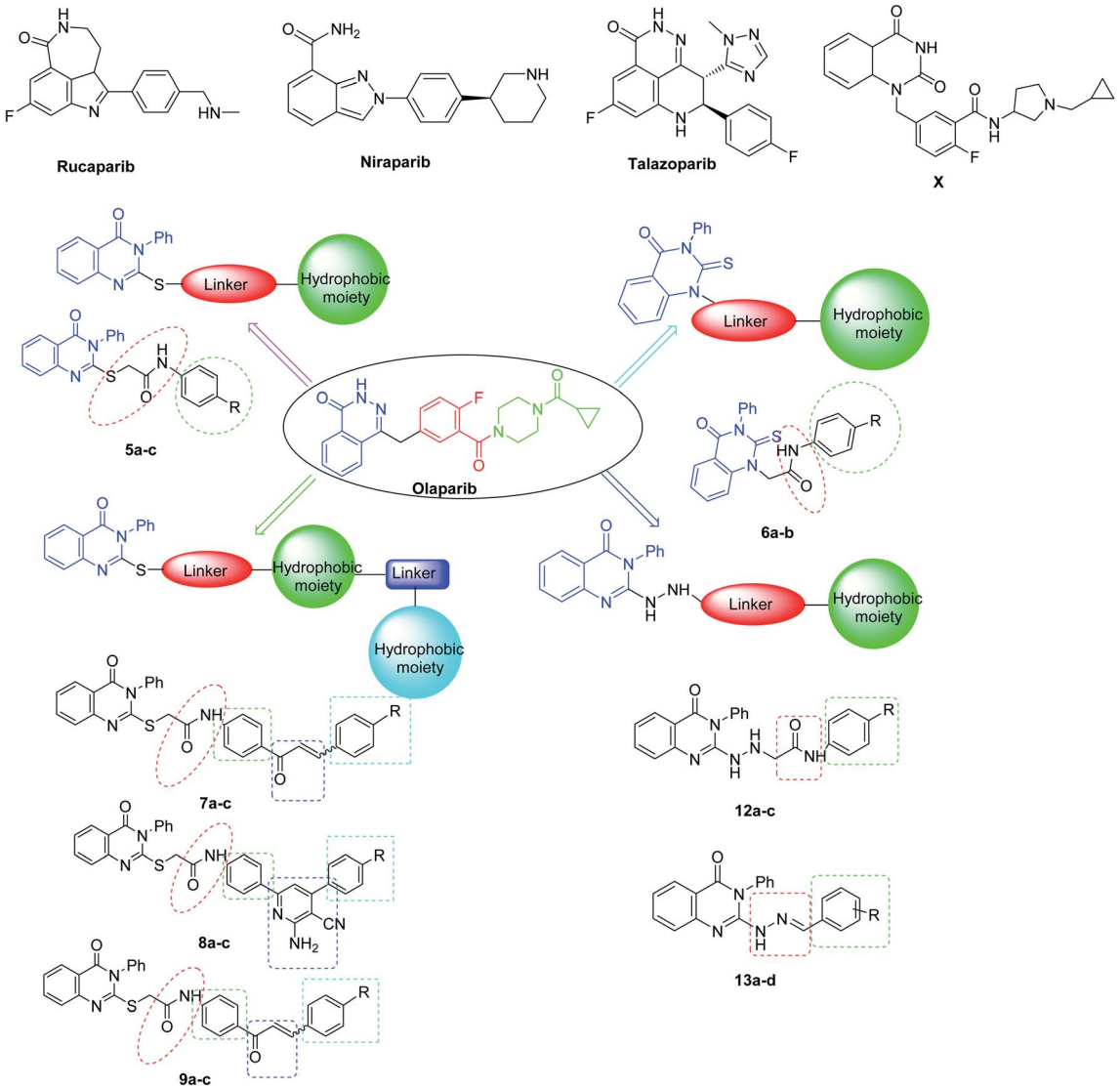

Fig. 1 Chemical structures of the approved PARP-1 inhibitors (**Rucaparib**, **Niraparib**, and **Talazoparib** and **Olaparib**) and the target derivatives [(**5a–c**), (**6a–c**), (**7a,b**), (**8a–c**), (**9a–c**), (**12a–c**), and (**13a–c**)].

Table 1 Comparison between the conventional and microwave irradiation methods

	M. W		Conv.			M. W		Conv.	
Comp. no.	T^M (min)	Y^M (%)	T^c (min)	Y^c (%)	Comp. no.	T^M (min)	Y^M (%)	T^c (min)	Y^c (%)
5a	3	85.57	360	67.44	**8c**	6	88.45	540	69.57
5b	4	93.53	480	59.71	**9a**	4	91.43	480	54.44
5c	3	86.51	420	69.55	**9b**	4	92.34	420	65.59
6a	3	85.47	360	57.73	**9c**	4	91.39	480	68.49
6b	6	93.50	480	59.81	**12a**	4	89.60	360	63.47
6c	3	86.58	420	69.66	**12b**	6	88.47	540	54.55
7a	3	85.51	360	57.65	**12c**	4	91.44	480	65.59
7b	4	93.61	480	59.60	**13a**	4	92.54	420	67.66
7c	3	86.59	420	63.63	**13b**	5	88.50	460	66.58
8a	4	91.48	480	57.65	**13c**	4	89.49	360	67.45
8b	4	89.55	360	68.54	**13d**	6	88.48	340	68.46

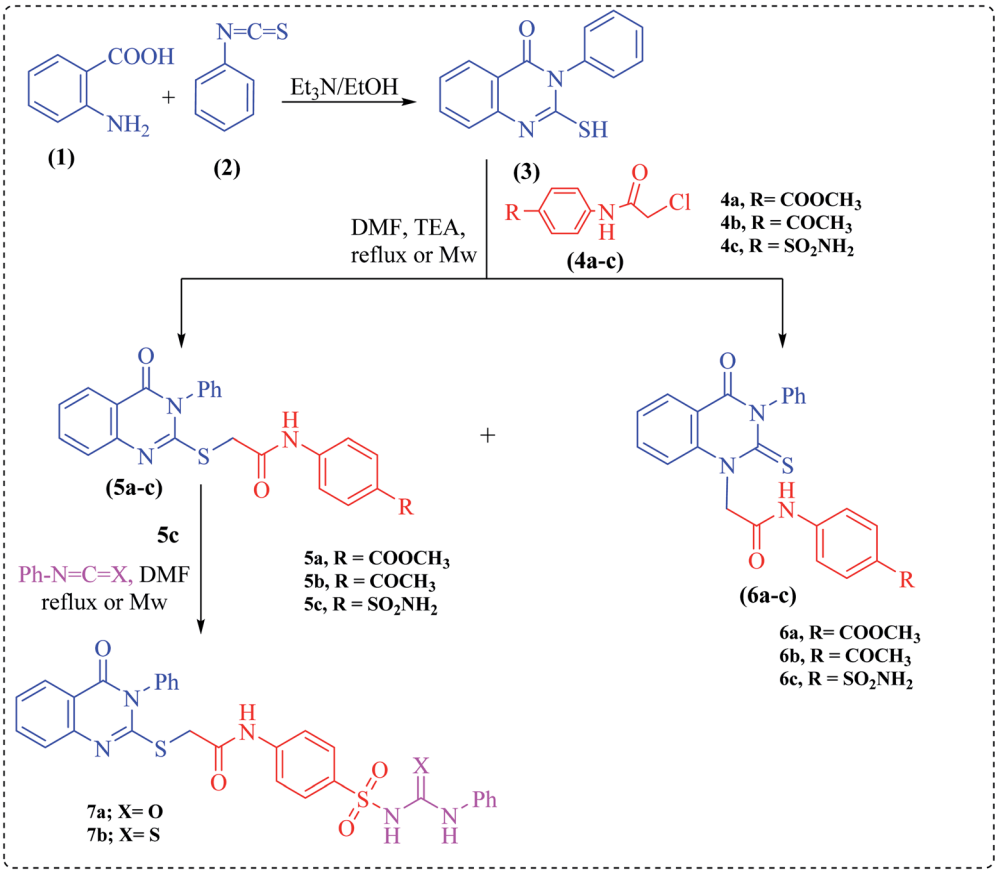

Scheme 1 Synthesis of compounds 3–7.

3. Results and discussion

3.1. Chemistry

Our continuing efforts were directed toward the design and construction of new heterocyclic compounds with anticipated pharmacological activities[19,20] using green chemistry tools.[21,22] Therefore, in this study, we report a highly efficient method for the synthesis of target potentially bioactive quinazoline derivatives (**3–14**) using both conventional and microwave irradiation methods, as outlined in Schemes 1–3. It was observed that the microwave approach proved to be extremely fast, providing good to excellent yields (80–93%) as compared with the

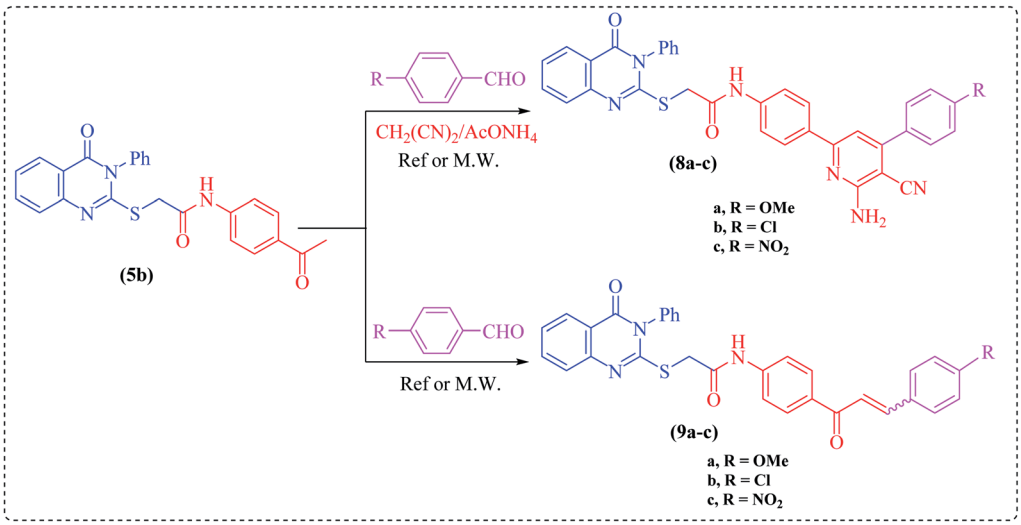

Scheme 2 Synthesis of compounds 8–9.

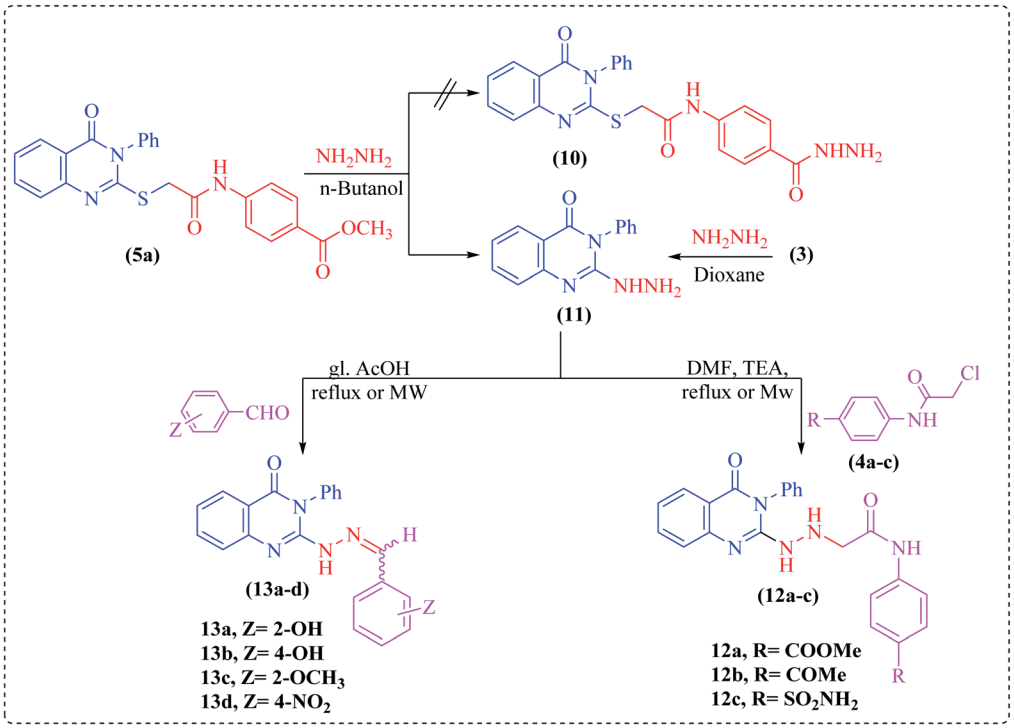

Scheme 3 Synthesis of compounds 11–13.

conventional method (54–68%). Here, the most noticeable advancement was the speed at which the reaction proceeded as the reaction was completed within 4–6 min, being 40–42 times faster than the conventional method. These results are summarized in Table 1.

Herein, the key starting material, 2-mercapto-3-phenylquinazolinone **3**, was prepared *via* treating anthranilic acid with phenyl isothiocyanate in boiling ethanol containing a few drops of triethylamine.[23] 2-Chloro-*N*-(substituted)acetamide derivatives (**4a–c**) were prepared by treatment of methyl 4-aminobenzoate, 4-aminoacetophenone and sulfanilamide with chloroacetyl chloride under basic conditions at room temperature.

Alkylation of quinazoline **3** with 2-chloro-*N*-(substituted) acetamide derivatives **4a–c** was carried out afterwards to achieve both *S*-alkylated and *N*-alkylated products **5a–c** and **6a–c**, respectively (Scheme 1). The structures of compounds **5a–c**, and **6a–c** were inferred from their elemental analyses, IR, NMR and MS spectra and were compatible with the proposed structures. Thus, the IR spectra exhibited two absorption bands at around ν = 3414 and 3228 cm^{-1} due to NH groups and two strong carbonyl absorption bands ranging from 1725–1685 cm^{-1}. Their ^1H NMR spectra provided exchangeable singlets of NH groups around the region δ = 13.00–10.30 ppm.

In turn, the sulfonamide derivative **5c** was further reacted with phenyl isocyanate or phenyl isothiocyanate in DMF under microwave irradiation at 200 W power for 2 min to afford urea or thiourea derivatives **7a** and **b**, respectively (Scheme 1). The structures of **7a** and **b** were deduced by the absence of the NH_2

Table 2 *In vitro* inhibitory activity of the synthesized compounds against PARP-1[a]

Compd	IC_{50} (nM)	Compd	IC_{50} (nM)
Olaparib	30.38 ± 1.61	**9a**	101.6[b] ± 5.88
5a	336.0[b] ± 13.08	**9b**	174.3[b] ± 8.72
5b	218.3[b] ± 10.34	**9c**	313.7[b] ± 15.35
5c	354.1[b] ± 18.28	**12a**	39.07 ± 3.89
6a	55.96 ± 2.95	**12b**	89.69[b] ± 5.67
6b	64.67 ± 3.38	**12c**	27.89 ± 3.45
7a	128.4[b] ± 8.57	**13a**	102.3[b] ± 6.84
7b	79.06[b] ± 4.31	**13b**	44.16 ± 3.12
8a	32.49 ± 2.64	**13c**	45.64 ± 2.86
8b	154.66[b] ± 8.76	**13d**	485.3[b] ± 26.0
8c	403.2[b] ± 21.27		

[a] Data are displayed as mean ± S. E. M. n = 3 (three independent repeats). Statistical analysis was carried out using one-way ANOVA followed by Dunnett *post hoc* test. [b] Statistically significant from **Olaparib** at $p < 0.05$.

Table 3 Effect of compounds **12a** and **12c** on cell cycle progression in MCF-7 cells

	DNA content%			
Compound	% G0–G1	% S	% G2–M	% Pre G1
12a/MCF7	38.51	23.43	38.06	26.55
12c/MCF7	43.28	33.23	23.49	19.31
Stauroporine/MCF7	37.19	26.22	36.59	31.74
cont. MCF7	59.26	34.17	6.57	1.57

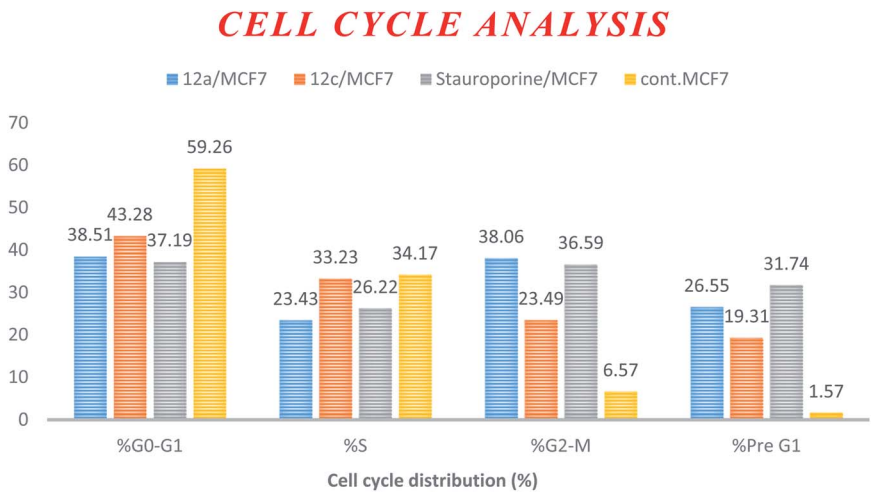

Fig. 2 Cell cycle analysis and apoptosis effect in the MCF-7 cell line when treated with compounds **12a** and **12c**.

absorption band characteristic for compound **5c** in the IR and ^{1}H NMR spectra.

One-pot multicomponent reaction of the acetyl derivative **5b** with malononitrile and the appropriate aromatic aldehydes, namely 4-methoxy-, 4-chloro- or 4-nitrobenzaldehyde, in dioxane containing ammonium acetate under microwave irradiation at 200 W power for 2–3 min furnished the corresponding enaminonitrile derivatives, namely *N*-(4-(6-amino-4-(4-substituted phenyl)-5-cyanopyridin-2-yl)phenyl)-2-(4-oxo-3-phenyl-3,4-dihydroquinazolin-2-ylthio)-acetamide (**8a–c**), respectively. The structures of these compounds were established based on their analytical and spectral data. Thus, the IR spectra showed the existence of cyano group absorption bands at around $\nu = 2226–2216$ cm^{-1}. Their ^{1}H NMR spectra exhibited singlets in the region of $\delta = 13.00–10.30$ ppm, assigned to two exchangeable protons, which are attributed to the NH_2 protons of the pyridine moiety.

On the other hand, chalcones and their derivatives are known to be important intermediates in organic synthesis because they serve as building block synthons for a wide variety

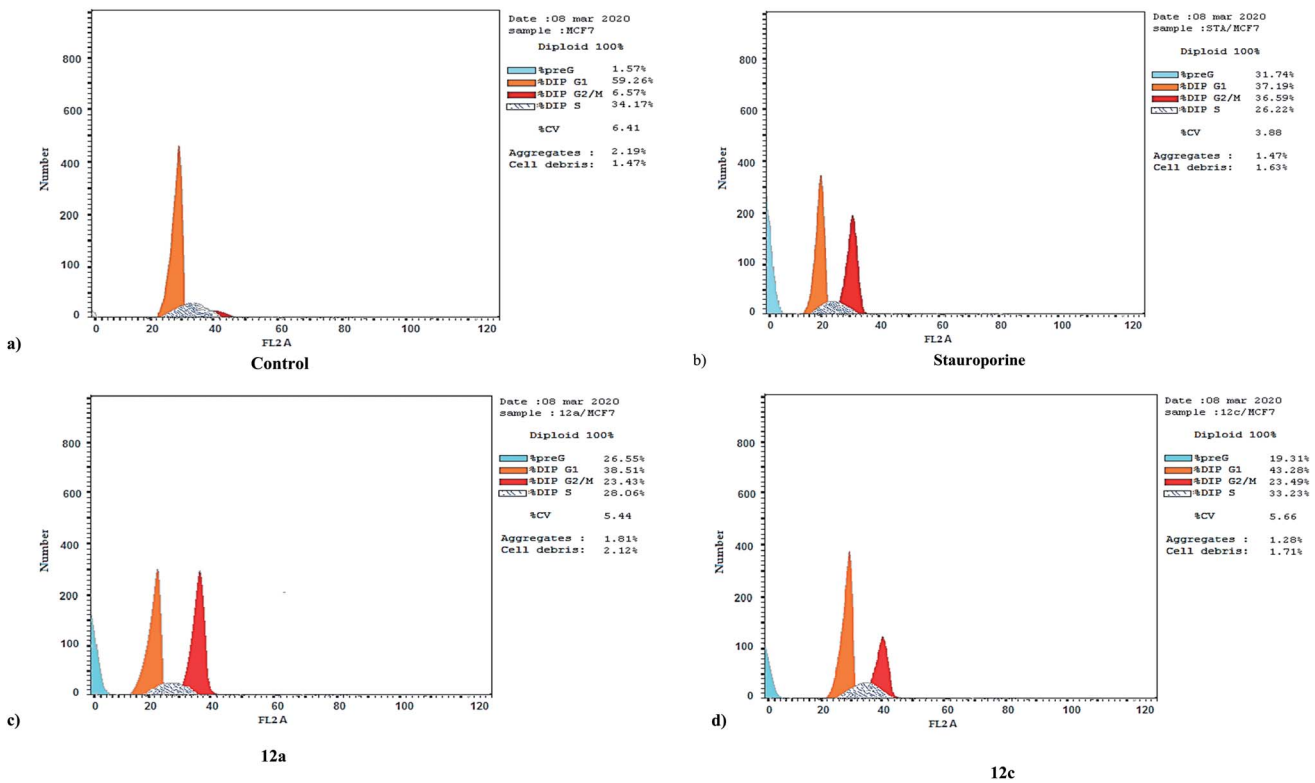

Fig. 3 MCF-7 cell distribution upon treatment with compounds **12a** and **12c**.

of heterocyclic compounds which are of physiological importance.[24–26] The presence of an enone functionality in the chalcone moiety confers biological activity, like anti-inflammatory,[27] antifungal,[28] antioxidant,[29] antimalarial,[30] antituberculosis,[31] anti-HIV[32] and antitumor[33] activities. Indeed, Claisen–Schmidt condensation of ketone **5b** with the same aromatic aldehydes as in Scheme 2, in the presence of NaOH, under microwave irradiation, afforded the corresponding α,β-unsaturated ketones (chalcones), namely *N*-(4-(3-(4-substituted phenyl)acryloyl) phenyl)-2-(4-oxo-3-phenyl-3,4-dihydroquinazolin-2-ylthio) acetamide (**9a–c**), respectively. The structures of these chalcones were substantiated by their analytical and spectral data. The ^{1}H NMR spectra displayed the absence of the singlet of methyl protons in compound **5b** (*cf.* Experimental).

Noteworthily, hydrazinolysis of compound **5a** using hydrazine hydrate in *n*-butanol under reflux conditions failed to produce the expected hydrazide **10**, but afforded 2-hydrazinyl-3-phenylquinazoline derivative **11** (Scheme 3). The structure of **11** was confirmed by spectral data and by direct comparison with an authentic sample prepared by treating the starting quinazoline **3** with hydrazine hydrate in refluxing dioxane.[23] Subsequently, the reaction of hydrazinoquinazoline **11** with 2-chloro-*N*-acetamide derivatives **4a–c** in DMF containing two drops of triethylamine under microwave irradiation furnished the hydrazinylacetamide derivatives, namely *N*-(4-substituted phenyl)-2-(2-(4-oxo-3-phenyl-3,4-dihydroquinazolin-2-yl) hydrazinyl)-acetamide (**12a–c**). The structures of all newly synthesized compounds were confirmed on the basis of spectral and elemental analyses, which were in full agreement with the proposed structures.

Finally, condensation of compound **11** with different aromatic aldehydes, namely 2-hydroxy-, 4-hydroxy-, 2-methoxy-, or 4-nitrobenzaldehyde under microwave irradiation or using the conventional method in glacial acetic acid produced the corresponding hydrazone derivatives **13a–d** (Scheme 3). In the ^{1}H NMR spectra of all compounds, a singlet peak corresponding to the imine proton (N=CH) was observed as a sharp singlet downfield of the aryl proton peaks, as well as a broad singlet for the NH group, while the singlet of NH_2 protons was absent (*cf.* Experimental).

3.2. Biological evaluation

3.2.1. *In vitro* PARP-1 inhibitory assay. The synthesized compounds were evaluated for their PARP-1 inhibitory activity. As shown in Table 2, the synthesized compounds displayed a wide range of inhibitory activities against PARP-1 in the nanomolar range with IC_{50} values ranging from 27.89 nM to 485.3 nM compared to the reference drug **Olaparib** (30.38 nM). Interestingly, compound **12c** was the most potent (27.89 nM) as a PPAR-1 inhibitor in comparison to **Olaparib** (30.38 nM). Moreover, compounds **6a**, **6b**, **8a**, **12a**, **13b** and **13c** did not show a statistically significant difference ($p < 0.05$) in IC_{50} value compared to **Olaparib**. The rest of the compounds were less potent, as evidenced by the statistically significant differences in comparison to **Olaparib**. In compounds **5a–c**, the ketone group on the phenyl was more tolerated than the ester group,

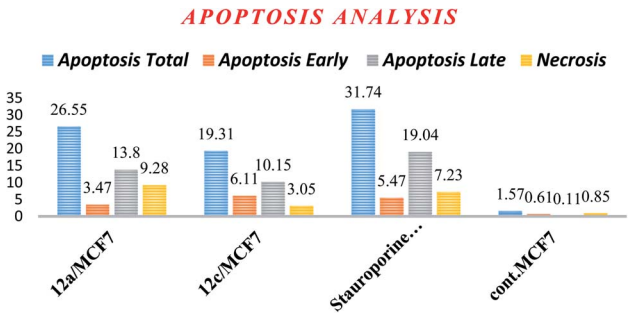

Fig. 4 Percentage of cell death induced by compounds **12a** and **12c** in MCF-7 cells.

which was better than the sulfonamide substitution, suggesting that hydrophobic residues in this position are preferred.

The higher potency of compounds **6a–b** when compared to compounds **5a–b** revealed that substitution at position-1 of the quinazoline was better than at position-2. Also, the extension of compound **5c** to give compounds **7a** and **7b** significantly increased the potency, suggesting extra hydrophobic binding in the AD site of PARP-1. In compounds **8a–c**, the methoxy derivative displayed higher activity than the chloro and nitro derivatives, suggesting that the presence of an electron donating group is more preferred than an electron withdrawing group. This was also observed in compounds **9a–c**. Interestingly, series **12a–c** showed very good potency in comparison to **Olaparib** with the sulfonamide derivative **12c** showing the highest activity among all of the synthesized compounds. Of the hydrazone derivatives **13a–d**, compound **13b** showed higher activity then **13a**, suggesting that substitution in position-4 of the phenyl ring is better than at position-2. Also, the methoxy derivative **13c** showed better potency than the hydroxyl derivative **13a** and the nitro substitution in **13d** greatly decreased the potency, suggesting that electron donating groups were preferred over electron withdrawing groups.

3.2.2. Cell cycle analysis. To understand more the impact of compounds **12a** and **12c** on cancer cell growth inhibition, their effect on cell cycle distribution and apoptosis induction was assessed using MCF-7 cells according to the method outlined.[34,35] In the present work, the MCF-7 cell line was treated with compound **12a** and **12c** at a concentration equal to 10 μg mL^{-1} for 24 h. As shown in Table 3, Fig. 2 & 3, the percentage of MCF-7 cells in G2/M phase markedly increased from 6.57% to

Table 4 Apoptosis and necrosis percent induced by compounds **12a** and **12c** in MCF-7 cells

	Apoptosis			
	Total	Early	Late	Necrosis
12a/MCF7	26.55	3.47	13.8	9.28
12c/MCF7	19.31	6.11	10.15	3.05
Stauroporine/MCF7	31.74	5.47	19.04	7.23
cont. MCF7	1.57	0.61	0.11	0.85

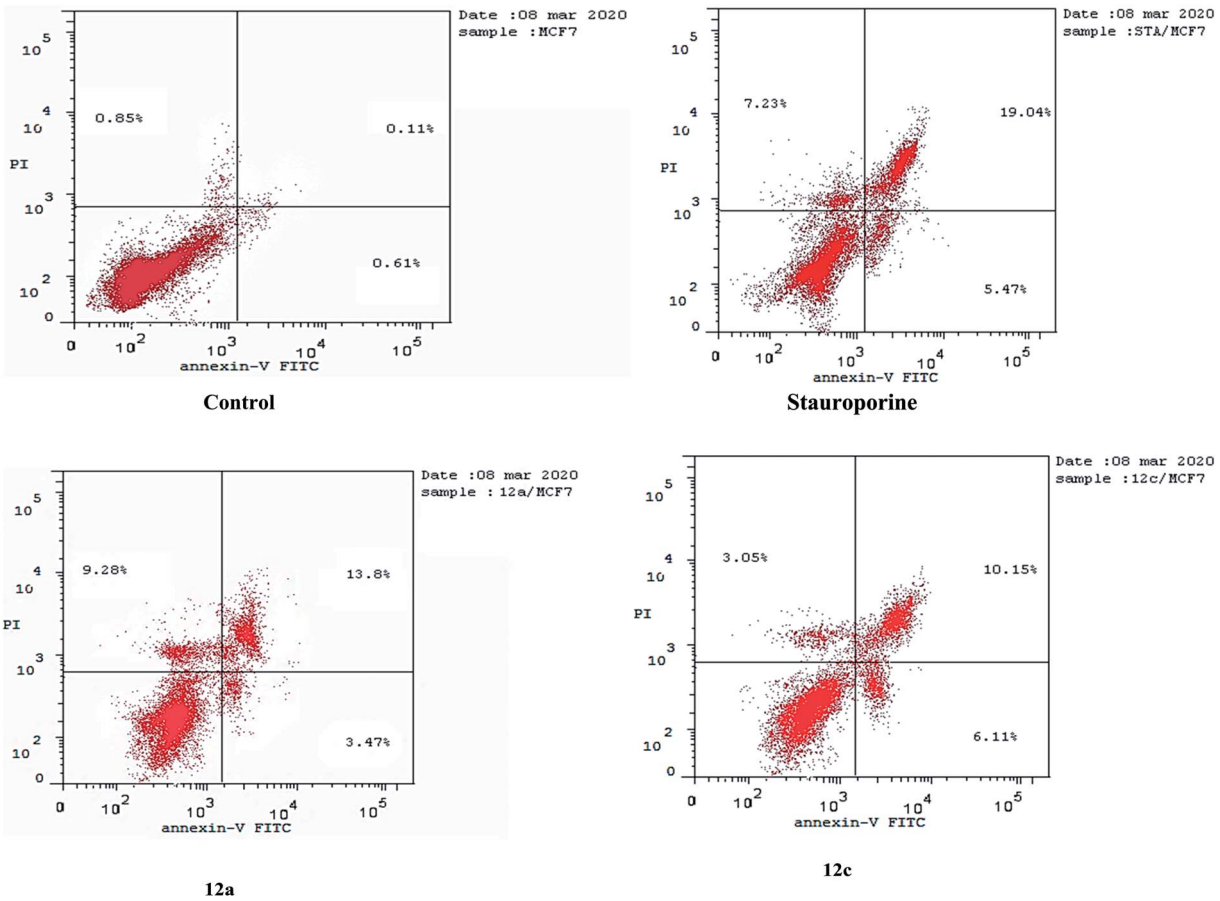

Fig. 5 Apoptosis induced in MCF-7 cells by compound **12a** and **12c**.

38.06% and 23.49% upon treatment with compound **12a** and **12c**, respectively. The percentage of MCF-7 cells in G1 phase decreased from 59.26% in the control to 38.51% and 43.28%, respectively, indicating that compounds **12a** and **12c** caused cell growth arrest at the G2/M phase (Fig. 4).

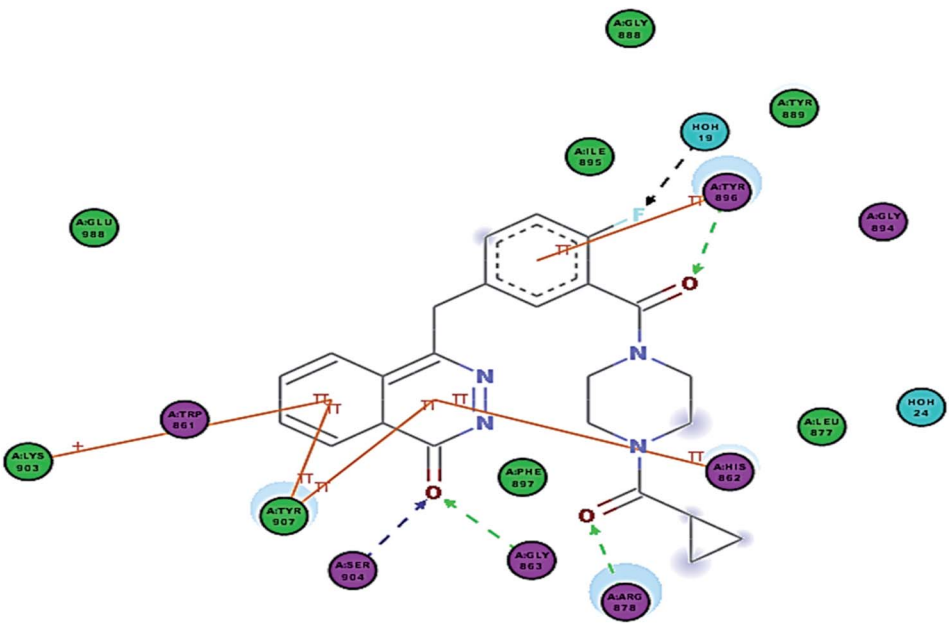

Fig. 6 2D interaction diagram showing **Olaparib** (lead compound) docking pose interactions with the key amino acids in the PARP-1 active site.

Table 5 The docking binding free energies of the synthesized compounds with PARP-1, forming hydrogen bonding and cationic-π interactions

Compd	ΔG kcal mol^{-1}	No. of hydrogen bonding	No. of cationic-π interactions
5a	−51.47	4 (TYR907, GLY863, TYR896, ARG878)	3 (TYR907, HIS862, LYS903)
5b	−53.18	4 (TYR907, HIS862, TYR896, ARG878)	3 (TYR907, HIS862, LYS903)
5c	−51.30	6 (TYR907, GLY863, HIS862, TYR896, ARG878, TYR907)	3 (TYR907, HIS862, LYS903)
6a	−57.87	5 (GLY863, HIS862, TYR896, ARG878, ARG878)	3 (TYR907, HIS862, LYS903)
6b	−55.23	5 (TYR907, GLY863, HIS862, TYR896, ARG878)	3 (TYR907, HIS862, LYS903)
7a	−58.20	7 (TYR907, GLY863, HIS862, GLY888, ALA880, ARG878, ARG878)	3 (TYR907, HIS862, ARG878)
7b	−58.43	6 (TYR907, GLY863, HIS862, GLY888, ALA880, ARG878, ARG878)	3 (TYR907, HIS862, ARG878)
8a	−62.52	6 (TYR907, GLY863, HIS862, TYR896, ARG878, ASN868)	3 (TYR907, HIS862, HIS862)
8b	−57.54	5 (TYR907, GLY863, HIS862, TYR896, ARG878)	3 (TYR907, HIS862, HIS862)
8c	−54.18	5 (TYR907, GLY863, HIS862, TYR896, ARG878)	3 (TYR907, HIS862, HIS862)
9a	−61.58	6 (TYR907, GLY863, HIS862, GLY894, ARG878, ASN868)	3 (TYR907, HIS862, LYS903)
9b	−61.10	4 (TYR907, GLY863, GLY894, ARG878)	3 (TYR907, HIS862, LYS903)
9c	−58.25	5 (TYR907, GLY863, HIS862, GLY894, ARG878)	3 (TYR907, HIS862, LYS903)
12a	−59.61	9 (TYR907, SER904, GLY863, HIS862, GLY888, TYR889, TYR896, ARG878, ARG878)	3 (TYR907, HIS862, LYS903)
12b	−58.01	8 (TYR907, SER904, GLY863, HIS862, GLY888, TYR889, TYR896, ARG878)	3 (TYR907, HIS862, LYS903)
12c	−59.56	8 (TYR907, SER904, GLY863, HIS862, GLY888, TYR889, TYR896, ARG878)	3 (TYR907, HIS862, LYS903)
13a	−53.14	5 (TYR907, TYR907, GLY863, HIS862, GLY888)	3 (TYR907, HIS862, LYS903)
13b	−55.98	6 (TYR907, TYR907, GLY863, HIS862, ALA880, ARG878)	3 (TYR907, HIS862, LYS903)
13c	−55.01	5 (TYR907, TYR907, GLY863, HIS862, TYR896)	3 (TYR907, HIS862, LYS903)
13d	−50.56	5 (TYR907, TYR907, GLY863, HIS862, TYR889)	3 (TYR907, HIS862, LYS903)
Olaparib	−60.60	4 (GLY863, SER904, TYR896, ARG878)	3 (TYR907, HIS862, LYS903, TYR896)

3.2.3. Annexin V-FITC apoptosis assay. To examine the involvement of apoptosis in the antiproliferative action of the tested compounds **12a** and **12c**, an Annexin V and PI double staining assay was performed.[36] In this assay, MCF-7 cells were incubated with 2.5 μM of each compound for 24 h. The percentage of apoptotic cells was determined and the stained cells were detected by flow cytometry. The results are reported in Table 4, Fig. 5 & 6. The results revealed that compound **12a** induced a total apoptotic effect equal 26.55% and **12c** showed an effect equal to 19.31%, which were more than the control (1.57%) and comparable to that of Staurosporine. In detail, compounds **12a** and **12c** obviously induced early apoptosis by 3.47% and 6.11%, respectively, and they enhanced late apoptosis by 13.8% and 10.15%, respectively, when compared with the untreated control MCF-7 cells (0.61% and 0.11%, respectively).

3.3. *In silico* studies

3.3.1. Molecular docking. In order to explore the binding mode of the designed quinazoline derivatives, we obtained and analyzed the docked structures of the synthesized compounds within the catalytic site of PARP-1 and compared it with that of **Olaparib**. As shown in Table 5, the docking results were consistent with the PARP-1 enzyme assay, where the potent compounds showed good affinity to the enzyme as illustrated by their docking score.

In **Olaparib**, the phthalazinone scaffold occupies the NI-site and the carbonyl group of the ring interacts with Gly863 and Ser904 through characteristic hydrogen bonds, and it also shows π–π stacking interactions with Tyr907 and His862. Interestingly, the 2-fluorobenzamide linker formed a π–π interaction with Tyr896 and a hydrogen bond with the backbone of Tyr896. Also, the carbonyl on the piperazine ring formed a H-

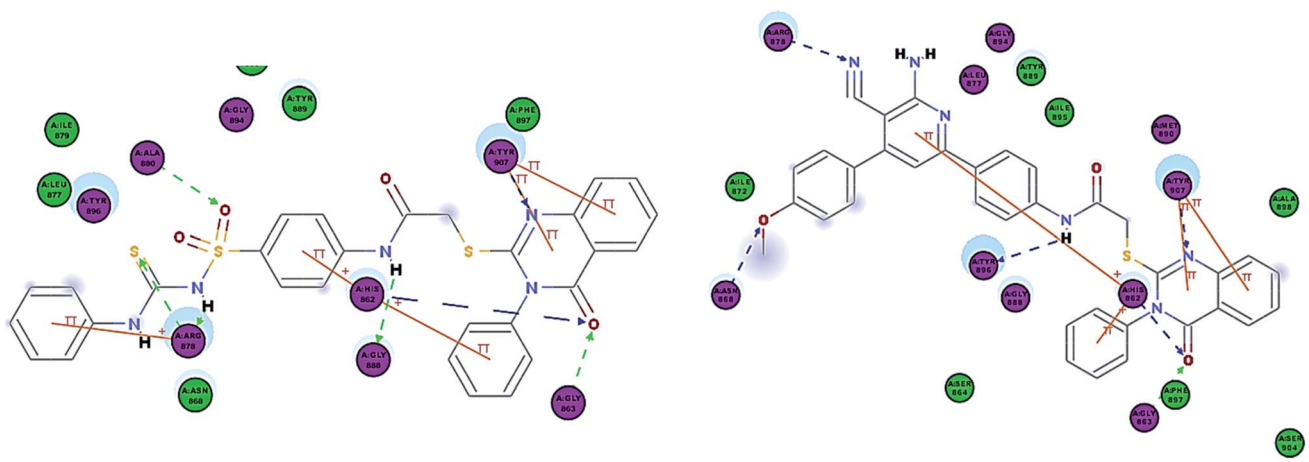

Fig. 7 2D interaction diagram of **7b** in the active site of PARP-1 and 2D interaction diagram of **8a** in the active site of PARP-1.

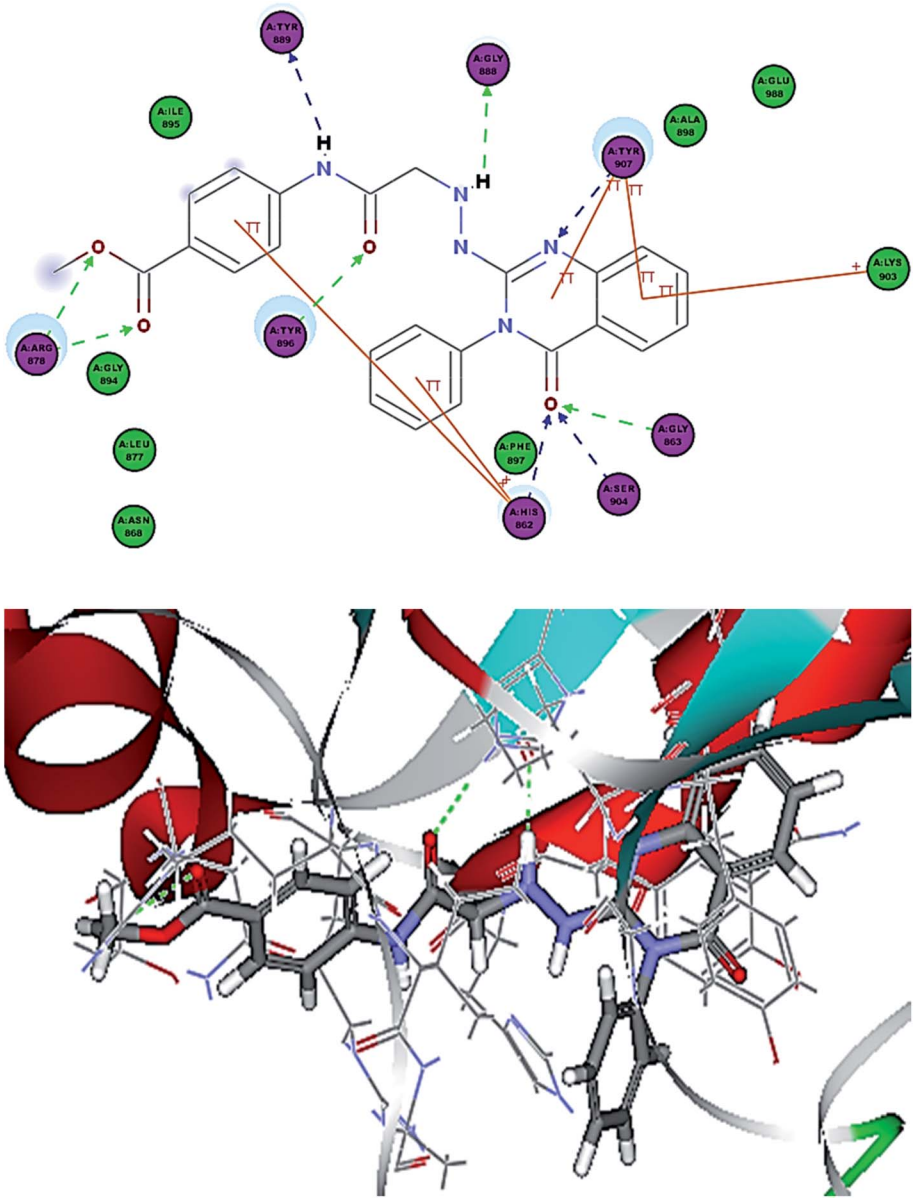

Fig. 8 2D interaction diagram of **12a** in the active site of PARP-1 and 3D interaction diagram of **12a** in the active site of PARP-1.

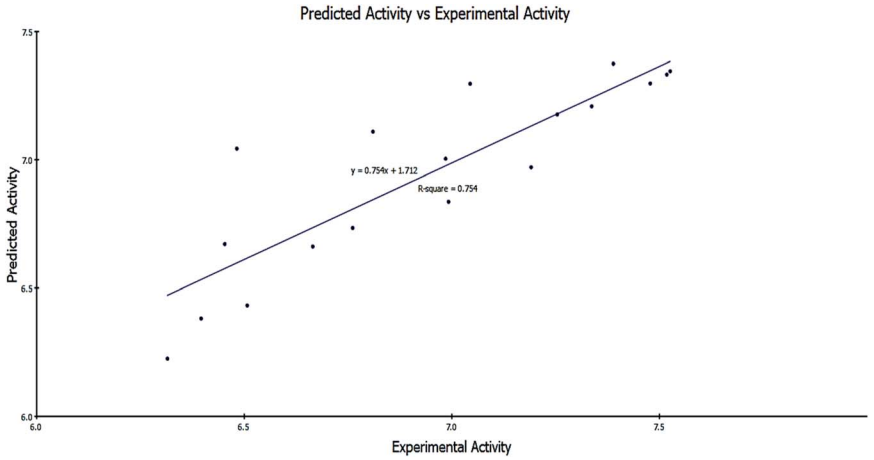

Fig. 9 Predicted activity *versus* experimental activity ($-\log IC_{50}$) values of the training set according to eqn (1) ($r^2 = 0.754$).

Table 6 Experimental activity of the synthesized compounds against the predicted activity according to the model equation

Compd	Experimental activity ($-\log IC_{50}$)	Predicted activity ($-\log IC_{50}$)	Residual
5a	6.482	7.043	−0.561
5b	6.665	6.662	0.003
5c	6.453	6.671	−0.218
6a	7.254	7.176	0.078
6b	7.191	6.970	0.221
8a	7.478	7.298	0.18
8b	6.810	7.109	−0.299
8c	6.396	6.381	0.015
9a	6.992	6.836	0.156
9b	6.761	6.734	0.027
9c	6.507	6.432	0.075
12a	7.389	7.375	0.014
12b	7.044	7.297	−0.253
12c	7.526	7.346	0.180
13a	6.985	7.004	−0.019
13c	7.337	7.209	0.128
13d	6.315	6.224	0.091
Olaparib	7.518	7.333	0.185
7a[a]	6.886	6.947	−0.061
7b[a]	7.103	7.335	−0.232
13b[a]	7.348	7.196	0.152

[a] **7a**, **7b**, and **13b** were used for external validation through calculating their predicted activity from the QSAR model constructed using the training set.

bond with Arg878. The cyclopropyl group was nicely inserted into a deep hydrophobic pocket.

Interpretation of the docking results showed that the majority of the designed compounds fit into the active site of PARP-1; most of them displayed comparable docking scores and binding modes similar to that of **Olaparib** and were able to reproduce the main interactions observed in **Olaparib**.

As expected, the quinazoline scaffold occupied the NI site, where the carbonyl group formed two hydrogen bonds with His862 and Gly863. Also, the N of the ring formed a hydrogen bond with Tyr907 in all of the synthesized compounds, except for **6a** and **6b** which formed a hydrogen bond with Tyr907 but *via* the ring sulfur. The quinazoline scaffold also showed π–π stacking interactions with Tyr907 and His862 previously observed in **Olaparib**. Additionally, it formed a π-cation interaction with Lys903 (Fig. 7).

In compounds **5a–c** and **6a–b**, the carbonyl group of the amide formed a hydrogen bond with Tyr896 similar to that of **Olaparib** and their terminal groups formed a hydrogen bond with Arg878 similar to that of **Olaparib**. When comparing this group of compounds, **6a** and **6b** showed better docking energies in comparison to **5a** and **5b**, indicating that the substitution on the nitrogen is better than that on the sulfur of the quinazolinone ring and this was also consistent with their enzyme assay results.

Interestingly, compounds **7a** and **7b** showed extra interactions; the amino group forms a hydrogen bond with Gly888 and the S=O group forms a hydrogen bond with Ala880 (Fig. 8), and this explained the increase in potency in comparison to **5c**.

Compounds **8a–c** showed the same interactions as **5a–b** but Arg878 formed a hydrogen bond with the cyano group instead of the terminal substitution (Fig. 8). The methoxy group in **8a** and **9a** shows an extra hydrogen bond with Asn868, which might explain their higher potency than **8b–c** and **9b–c**, respectively, suggesting that methoxy substitution was better than chloro and nitro groups.

Compounds **12a–c** showed additional interactions through hydrogen bonds between the NH of the hydrazine formed and Gly888, and between the amide NH and Tyr889. Additionally, the ester function or sulfonamide moieties form two H bonds with Arg878, which could explain the high potency of this series (Fig. 9). Compounds **13a–c** showed the essential interactions with the NI site, but they lacked the hydrogen bond with the linker. Moreover, different substitutions on the terminal phenyl ring formed different interactions with various amino acids in the AD site of the enzyme. The presence of a hydroxyl group in position-4 gave the best docking score and the hydroxyl group

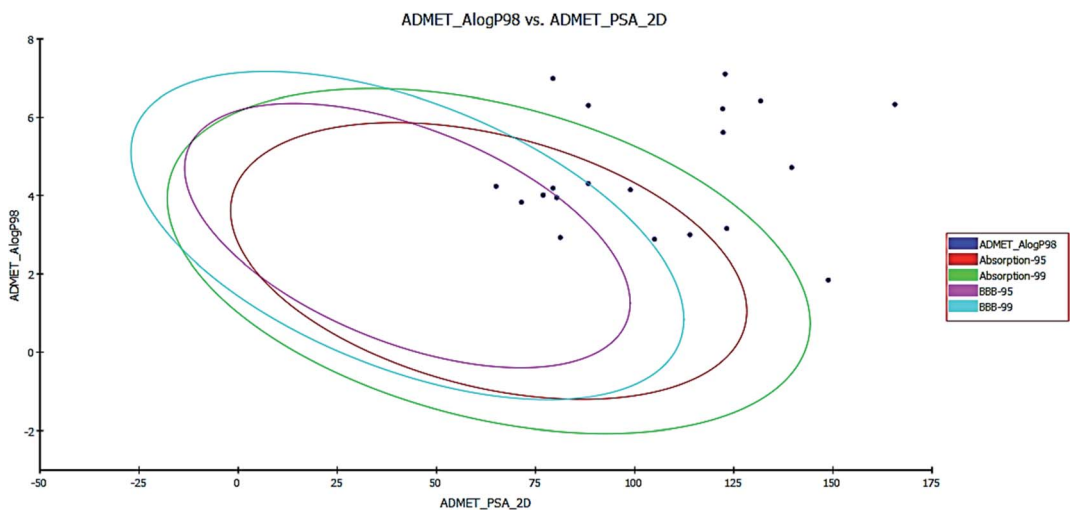

Fig. 10 ADMET plot for the newly synthesized compounds.

Table 7 Computer aided ADMET screening of the synthesized compounds

Cpd ID	BBB_Lev[a]	Absorp_Lev[b]	AQ SOlLEV[c]	Hepatox[d]	Hepatox prob[e]	CYP2D6[f]	CYP2D6Prob[g]	PPB_Lev[h]	AlogP98[i]	ADEM_PSA_2D[j]
5a	2	0	2	1	0.841	1	0.732	2	4.305	88.318
5b	2	0	2	1	0.821	1	0.712	2	4.189	79.388
5c	4	1	2	1	0.827	0	0.485	2	3.154	123.22
6a	2	0	2	1	0.94	0	0.495	2	3.944	80.347
6b	2	0	2	1	0.927	1	0.633	2	3.828	71.417
7a	4	2	2	1	0.88	0	0.297	2	4.717	139.61
7b	4	2	1	1	0.874	0	0.297	2	5.616	122.31
8a	4	2	1	1	0.952	0	0.346	2	6.419	131.75
8b	4	3	1	1	0.953	0	0.316	2	7.1	122.83
8c	4	3	1	1	0.951	0	0.316	2	6.33	165.64
9a	4	2	1	1	0.821	0	0.366	2	6.305	88.318
9b	4	2	1	1	0.814	0	0.475	2	6.986	79.388
9c	4	2	1	1	0.834	0	0.425	2	6.216	122.21
12a	4	0	2	1	0.814	1	0.613	2	2.995	113.93
12b	4	0	2	1	0.834	1	0.623	2	2.88	105.01
12c	4	2	2	1	0.827	0	0.475	2	1.845	148.84
13a	2	0	2	1	0.953	1	0.603	2	4.011	76.925
13b	2	0	2	1	0.973	1	0.742	2	4.011	76.925
13c	1	0	2	1	0.933	1	0.871	2	4.236	65.04
13d	4	0	2	1	0.953	1	0.524	2	4.147	98.933

[a] Blood brain barrier level; 4 = undefined, 2 = medium penetration, 1 = high penetration. [b] Absorption level; 3 = very low absorption, 2 = low absorption, 1 = moderate absorption, 0 = good absorption. [c] Aqueous solubility level; 4 = optimal, 3 = good, 2 = low solubility, 1 = very low but soluble, 0 = extremely low. [d] Hepatotoxicity level; 1 = toxic, 0 = nontoxic. [e] Hepatotoxicity probability. [f] CYP2D6 inhibition; 1 = likely to inhibit, 0 = non inhibitor. [g] Cyp2D6 inhibition probability. [h] Plasma protein binding; 2 = more than 95%, 1 = more than 90%, 0 = less than 90%. [i] Lipophilicity descriptor; compounds must have log p value not greater than 5.0 to attain a reasonable probability of being well absorbed. [j] Polar surface area.

was involved in two hydrogen bond interactions, which explains why **13b** showed the best potency among this group.

3.3.2. QSAR study. A QSAR study was performed in order to understand the factors impacting the activity of the compounds. Experimental IC_{50} values for the compounds against PARP-1 were used, along with topological and geometrical descriptors to generate the following QSAR equation describing the best performing QSAR model.

$$-\log IC_{50} = 2.98977 + 1.06691 \times CHI\_V\_3\_C - 0.141044 \times Dipole\_mag + 6.03536 \times Jurs\_FPSA\_1 \quad (1)$$

Abbreviations used: $-\log IC_{50}$: the negative logarithmic value of the concentration required to produce 50% inhibition of MCF-7 cells. CHI_V_3_C: Kier & Hall valence-modified connectivity index. This index is a refinement of the molecular connectivity index that takes into account the electron configuration of the atoms.[37] Dipole_mag: 3D electronic descriptor that indicates the strength and orientation behavior of a molecule in an electrostatic field.[38] Jurs_FPSA_1: fractional charged partial surface area, which combines shape and electronic information to characterize molecules. The descriptors are calculated by mapping atomic partial charges on solvent-accessible surface areas of individual atoms.[39]

3.3.3. Validation of QSAR. The QSAR model was validated by employing leave one-out cross-validation, and calculating the predicted activity for the test set through running them as external test compounds in the constructed QSAR model using the "calculate molecular properties" protocol and selecting the model from the "Other" set, and the residuals between the experimental activities and those predicted by the QSAR study are presented in Table 6.

The regression values were as follows: $r^2 = 0.754$, $q^2 = 0.638$ and least-squared error = 0.0403.

It was clearly illustrated that the IC_{50} values predicated by our QSAR model were very close to those experimentally observed, indicating that this model can be used productively for the predication of more effective hits having the same skeletal framework.

3.3.4. *In silico* ADMET study. The pharmacokinetic properties of the synthesized compounds were predicted using the ADMET protocol in Accelrys Discovery Studio 2.5 software. The results of the ADMET study are presented as an ADMET-plot, which is a 2D plot drawn using the calculated PSA_2D and AlogP98 properties (Fig. 10).

In the BBB plot, most of the compounds except for **5a**, **5b**, **6a**, **6b**, **13a**, **13b** and **13c** fall outside of the 99% ellipse. Hence, these compounds may not be able to penetrate the blood brain barrier; hence, the chances of CNS side effects are predicted to be low. Meanwhile, for compounds **5a**, **5b**, **6a**, **6b**, **13a**, **13b** and **13c** there is a probability of causing CNS side effects.

In the HIA plot, most of the compounds fell inside the 99% ellipse, and are thus estimated to have good human intestinal absorption, except for **7a**, **7b**, **8a**, **8b**, **8c**, **9a**, **9b**, **9c** and **12c**, which show poor absorption. The ADME aqueous solubility level of most of the compounds was found to be 2 or 1, which indicates low aqueous solubility. The hepatotoxicity level of all compounds was 1. Hence, the compounds are predicted to possess hepatotoxicity. Further experimental studies are required to determine the hepatotoxic dose levels.

Most of the compounds are predicted as non-inhibitors of CYP2D6, and hence side effects (*i.e.* liver dysfunction) are not expected upon administration of these compounds, except for compounds **5a**, **5b**, **6b**, **12a**, **12b**, **13a**, **13b**, **13c** and **13d**.

The plasma protein-binding model predicts whether a compound is likely to be highly bound to carrier proteins in the blood. There is a high probability that the synthesized compounds bind to plasma proteins.

PSA is a key property that has been linked to drug bioavailability. Thus, passively absorbed molecules with PSA > 140 are thought to have low bioavailability. Most of the synthesized compounds have PSA values ranging from 65.04–139.61, and thus, they are predicted to present good passive oral absorption, except for compounds **8c** and **12c** which had a PSA of more than 140. The calculated parameters from the ADMET study are tabulated in Table 7 (*cf.* ESI†).

4. Conclusion

In this study, a new series of quinazolinone derivatives were designed and synthesized in an eco-friendly manner using a microwave-assisted method. All of the newly synthesized compounds were evaluated for their inhibitory activity towards PARP-1 and they showed inhibitory activity with IC_{50} values ranging from 29.78 nM to 483.75 nM. The most active compound **12c** (IC_{50} = 29.78 nM) showed the highest activity compared with **Olaparib** (IC_{50} = 30.27 nM).

Cell cycle analysis showed that **12a** and **12c** caused cell growth arrest at the G2/M phase in MCF-7 cells. Also, both compounds were shown to increase the programmed apoptosis compared with the control. Moreover, molecular docking of the most active compounds into the PARP-1 active site displayed a similar binding mode to **Olaparib**. A computational QSAR study was performed for the synthesized compounds. Collectively, these results revealed that some of the newly synthesized compounds could serve as hit potent PARP-1 inhibitors and anticancer agents.

5. Experimental section

5.1. Chemistry

5.1.1. General. All melting points were measured on GALLENKAMP melting point apparatus and were uncorrected. The microwave reactions were done by a Microsynth instrument type MA143 (Microwave flux). The IR spectra were recorded on a Pye-Unicam SP-3-300 infrared spectrophotometer (potassium bromide disks) and expressed in wave number (cm^{-1}). ^{1}H NMR spectra were run at 300 and 400 MHz, on a Varian Mercury VX-300 and Bruker Avance III NMR spectrometer, respectively. The ^{13}C NMR spectra (δ, ppm) were run at 100 MHz on a BRUKER NMR spectrometer (BRUKER, Manufacturing & Engineering Inc., Anaheim, CA, USA) at the Faculty of Pharmacy, Ain Shams University. TMS was used as an internal standard in deuterated dimethylsulfoxide (DMSO-d_6). Chemical shifts (δ) are quoted in ppm. The abbreviations used are as follows: s, singlet; d, doublet; m, multiplet. All coupling constant (J) values are given in hertz. The mass spectra were recorded on a Shimadzu GCMS-QP-1000EX mass spectrometer at 70 eV. Elemental analyses were performed on a CHN analyzer and all compounds were within ±0.4 of the theoretical values. The reactions were monitored by thin-layer chromatography (TLC) using TLC sheets coated with UV fluorescent silica gel Merck 60 F254 plates and were visualized using a UV lamp and different solvents as the mobile phase. All reagents and solvents were purified and dried by standard techniques. Compound **3** was previously reported.[23]

*3-Phenyl-2-thioxo-2,3-dihydroquinazolin-4(1H)-one (**3**).* A mixture of anthranilic acid **1** (1.37 g, 10 mmol), phenyl isothiocyanate **2** (1.79 mL, 15 mmol) and triethylamine (2 mL) in ethanol (30 mL) was heated under reflux for 4 h. The obtained white precipitate, while hot, was collected by filtration and recrystallized from an ethanol/dioxane mixture (1 : 1) to give quinazoline **3** as colorless crystals, mp 308–310 °C [lit.[23] 305–307 °C], IR (ν, cm^{-1}): 3264, 3135 (NH), 3070 (CH aromatic), 1663 (C=O). ^{1}H NMR (DMSO-d_6-D_2O) δ (ppm): 7.24–7.26 (m, 1H, Ar–H), 7.31–7.47 (m, 6H, Ar–H), 7.74–7.78 (m, 1H, Ar–H), 7.92–7.94 (m, 1H, Ar–H), 13.01 (br.s, 1H, NH, exchangeable). Anal. calcd for $C_{14}H_{10}N_2OS$ (254.3): C, 66.12; H, 3.96; N, 11.02. Found: C, 65.91; H, 3.90; N, 11.11%.

*Synthesis of the S- and N-alkylated quinazoline derivatives (**5a–c** and **6a–c**)*

(a) Conventional method. ***Method I.*** A mixture of compound **3** (5 mmol) and 2-chloro-*N*-(substituted phenyl)acetamide **4a–c** (5 mmol), namely methyl 4-(2-chloroacetamido)benzoate, *N*-(4-acetylphenyl)-2-chloroacetamide and 2-chloro-*N*-(4-sulfamoylphenyl)acetamide, in absolute ethanol (20 mL) containing freshly prepared anhydrous sodium acetate (5 mmol) was heated under reflux for 4 h. The precipitated solid, while hot, was filtered off and recrystallized from dioxane to afford the corresponding *N*-alkylated products **6a–c**, while the precipitate obtained after cooling the filtrate was collected and recrystallized from ethanol to give the *S*-alkylated products **5a–c**, respectively.

Method II. An equimolar mixture of compound **3** (5 mmol) and 2-chloro-*N*-(substituted phenyl)acetamide **4a–c** (5 mmol), namely methyl 4-(2-chloroacetamido)benzoate, *N*-(4-acetylphenyl)-2-chloroacetamide and 2-chloro-*N*-(4-sulfamoylphenyl)acetamide, in DMF (10 mL) containing two drops of triethylamine was stirred at room temperature for 10 h. The reaction mixture was poured onto ice-cooled water and acidified by dil. HCl (10%). The formed precipitate was filtered off and dried. This solid was a mixture of compounds **5a–c** and **6a–c**, which was separated by fractional recrystallization from ethanol to give compounds **5a–c**. The insoluble part in ethanol was recrystallized from dioxane to afford compounds **6a–c**.

(b) Microwave method. A mixture of compound **3** (5 mmol), the previously mentioned *N*-acetamido derivatives **4a–c** (5 mmol), namely methyl 4-(2-chloroacetamido)benzoate, *N*-(4-acetylphenyl)-2-chloroacetamide and 2-chloro-*N*-(4-sulfamoylphenyl)acetamide, 2 mL of DMF and two drops of triethylamine as a catalyst were added to the reaction vessel of the monomodal Emrys™ Creator microwave synthesizer and allowed to react under microwave irradiation at 200–400 W power for 2–

4 min. The automatic mode stirring helped with mixing and uniform heating of the reactants. The reaction vessel was cooled to room temperature. The solid mixture of compounds **5a–c** and **6a–c** was collected by filtration, washed with water, and separated by fractional crystallization from ethanol to give compounds **5a–c**. The insoluble part in ethanol was recrystallized from dioxane to afford compounds **6a–c**.

*Methyl 4-(2-((4-oxo-3-phenyl-3,4-dihydroquinazolin-2-yl)thio) acetamido)benzoate (**5a**).* White crystals, mp 190–192 °C, IR (ν, cm^{-1}): 3304 (NH), 3064 (CH aromatic), 2846 (CH aliphatic), 1699 (C=O). ^{1}H NMR (DMSO-d_6-D_2O) δ (ppm): 3.79 (s, 3H, CH_3), 4.09 (s, 2H, CH_2), 7.42–7.50 (m, 4H, Ar–H), 7.56–7.61 (m, 3H, Ar–H), 7.70–7.73 (dd, 2H, Ar–H, J_o = 10.8 Hz, J_m = 2 Hz), 7.76–7.80 (m, 1H, Ar–H), 7.88–7.91 (dd, 2H, Ar–H, J_o = 10.8 Hz, J_m = 2 Hz), 8.04–8.06 (dd, 1H, Ar–H, J_o = 8 Hz, J_m = 1.2 Hz), 10.68 (br.s, 1H, NH, exchangeable). MS, *m*/*z*, (%): 447 (M^+ + 2), (9.03%), 246 (M^+ + 1, 100%), 445 (33%). Anal. calcd for $C_{24}H_{19}N_3O_4S$ (445.49): C, 64.71; H, 4.30; N, 9.43. Found: C, 64.55; H, 4.21; N, 9.54%.

*N-(4-Acetylphenyl)-2-((4-oxo-3-phenyl-3,4-dihydroquinazolin-2-yl)thio)acetamide (**5b**).* White crystals, mp 160–162 °C, IR (ν, cm^{-1}): 3245 (NH), 3040 (CH aromatic), 1686, 1671 (C=O). ^{1}H NMR (DMSO-d_6-D_2O) δ (ppm): 2.47 (s, 3H, CH_3), 4.10 (s, 2H, CH_2), 7.42–7.50 (d, 4H, Ar–H), 7.56–7.60 (m, 3H, Ar–H), 7.72 (d, 2H, Ar–H, J = 8.8 Hz), 7.76–7.80 (m, 1H, Ar–H), 7.91 (d, 2H, Ar–H, J = 8.8 Hz), 8.04–8.06 (dd, 1H, Ar–H, J_o = 9.2 Hz, J_m = 1.2 Hz), 10.69 (br.s, 1H, NH, exchangeable). MS, *m*/*z*, (%): 429 (M^+, 7.04%), 386 (27.28%), 295 (100%). Anal. calcd for $C_{24}H_{19}N_3O_3S$ (429.49): C, 67.12; H, 4.46; N, 9.78. Found: C, 66.87; H, 4.38; N, 9.81%.

*2-((4-Oxo-3-phenyl-3,4-dihydroquinazolin-2-yl)thio)-N-(4-sulfamoylphenyl)acetamide (**5c**).* White crystals, mp 250–252 °C, IR (ν, cm^{-1}): 3311, 3245 (NH), 3070 (CH aromatic), 1669 (C=O). ^{1}H NMR (DMSO-d_6-D_2O) δ (ppm): 4.11 (s, 2H, CH_2), 7.21–7.75 (m, 9H, Ar–H), 7.76–7.80 (m, 1H, Ar–H), 7.93 (d, 2H, Ar–H, J = 7.2 Hz), 8.04–8.06 (dd, 1H, Ar–H, J_o = 8.8 Hz, J_m = 0.8 Hz), (br.s, 2H, NH_2, exchangeable), 13.02 (br.s, 1H, NH, exchangeable). Anal. calcd for $C_{22}H_{18}N_4O_4S_2$ (466.53): C, 56.64; H, 3.89; N, 12.01. Found: C, 56.44; H, 3.80; N, 11.93%.

*Methyl 4-(2-(4-oxo-3-phenyl-2-thioxo-3,4-dihydroquinazolin-1(2H)-yl)acetamido)benzoate (**6a**).* White crystals, mp >360 °C, yield: 25%. IR (ν, cm^{-1}): 3414 (NH), 3054 (CH aromatic), 2926 (CH aliphatic), 1664 (C=O). ^{1}H NMR (DMSO-d_6-D_2O) δ (ppm): 3.81 (s, 3H, CH_3), 4.19 (s, 2H, CH_2), 7.41–7.54 (m, 5H, Ar–H), 7.56–7.61 (m, 3H, Ar–H), 7.76–7.85 (m, 3H, Ar–H), 7.91 (d, 1H, Ar–H J = 8 Hz), 8.06 (d, 1H, Ar–H, J = 8 Hz), 11.21 (br.s, 1H, NH, exchangeable). ^{13}C NMR (100 MHz, DMSO-d_6) δ (ppm): 37.9, 52.3, 119.0 (3), 119.7, 124.6, 126.3 (2), 126.8, 130.0 (3), 130.3, 130.9 (3), 135.5, 136.0, 144.1, 147.4, 157.4, 161.2, 166.6. Anal. calcd for $C_{24}H_{19}N_3O_4S$ (445.49): C, 64.71; H, 4.30; N, 9.43. Found: C, 64.54; H, 4.22; N, 9.33%.

*N-(4-Acetylphenyl)-2-(4-oxo-3-phenyl-2-thioxo-3,4-dihydroquinazolin-1(2H)-yl)acetamide (**6b**).* White crystals, mp 220–222 °C, IR (ν, cm^{-1}): 3238 (NH), 3040 (CH aromatic), 1687, 1671 (C=O). ^{1}H-NMR (DMSO-d_6-D_2O) δ (ppm): 2.53 (s, 3H, CH_3), 4.14 (s, 2H, CH_2), 7.44–7.55 (m, 4H, Ar–H), 7.59–7.63 (m, 2H, Ar–H), 7.75–7.83 (m, 5H, Ar–H), 7.93 (d, 1H, Ar–H, J = 8 Hz), 8.08 (d, 1H, Ar–H, J = 8 Hz), 10.79 (br.s, 1H, NH, exchangeable). ^{13}C NMR (100 MHz, DMSO-d_6) δ (ppm): 26.7, 37.4, 118.7 (3), 120.0, 125.7, 126.3 (2), 127.1, 130.0 (4), 130.3, 131.9, 135.2, 136.0, 143.6, 147.1, 156.9, 160.7, 166.9, 196.7. Anal. calcd for $C_{24}H_{19}N_3O_3S$ (429.49): C, 67.12; H, 4.46; N, 9.78. Found: C, 66.89; H, 4.39; N, 9.67%.

*2-(4-Oxo-3-phenyl-2-thioxo-3,4-dihydroquinazolin-1(2H)-yl)-N-(4-sulfamoylphenyl) acetamide (**6c**).* White crystals, mp 264–266 °C, IR (ν, cm^{-1}): 3317, 3215 (NH, NH_2), 3074 (CH aromatic), 1671 (C=O). ^{1}H NMR (DMSO-d_6-D_2O) δ (ppm): 4.33 (s, 2H, CH_2), 7.26 (br.s, 2H, 2NH, exchangeable), 7.42–7.81 (m, 12H, Ar–H), 8.04–8.06 (dd, 1H, Ar–H, J_o = 8.8 Hz, J_m = 0.8 Hz), 10.85 (br.s, 1H, NH, exchangeable). Anal. calcd for $C_{22}H_{18}N_4O_4S_2$ (466.53): C, 56.64; H, 3.89; N, 12.01. Found: C, 56.44; H, 3.80; N, 11.93%.

*Reaction of **5c** with phenyl isocyanate/phenyl isothiocyanate: general procedure for the synthesis of compounds **7a** and **b***

(a) Conventional method. A mixture of the sulfonamide derivative **5c** (2 mmol) and phenyl isocyanate or phenyl isothiocyanate (2 mmol) in dioxane (20 mL) was heated under reflux for 8 h. The reaction mixture was then cooled and poured onto ice-cold water. The precipitated solid was collected and recrystallized from ethanol to produce urea/thiourea derivatives **7a** and **b**, respectively.

(b) Microwave method. A mixture of the sulfonamide derivative **5c** (2 mmol) and phenyl isocyanate or phenyl isothiocyanate (2 mmol) in DMF (2 mL) was added to the reaction vessel of the monomodal Emrys™ Creator microwave synthesizer and allowed to react under microwave irradiation at 200–400 W power for 2–4 min. The automatic mode stirring helped with mixing and uniform heating of the reactants. The reaction vessel was cooled to room temperature. The solid compound was collected by filtration, washed with water, and recrystallized from ethanol to give products **7a** and **b**, respectively.

*2-((4-Oxo-3-phenyl-3,4-dihydroquinazolin-2-yl)thio)-N-(4-(N-(phenylcarbamoyl) sulfamoyl)phenyl)acetamide (**7a**).* Beige crystals, mp 220–222 °C, IR (ν, cm^{-1}): 3330, 3286, 3194 (3NH), 3062 (CH aromatic), 1684, 1651 (C=O). ^{1}H NMR (DMSO-d_6-D_2O) δ (ppm): 4.12 (s, 2H, CH_2), 6.94–7.20 (m, 5H, Ar–$H_{phenyl\ ring}$), 7.29–7.48 (m, 6H, Ar–H), 7.57–7.80 (m, 5H, Ar–H), 7.82–8.09 (m, 2H, Ar–H quinazolinone), 9.23 (br.s, 2H, NH, exchangeable), 10.38 (br.s, 1H, NH, exchangeable). ^{13}C NMR (100 MHz, DMSO-d_6) δ (ppm): 37.6, 114.4, 118.5 (3), 119.6, 119.9, 122.0 (2), 123.7, 126.3, 126.4, 127.1, 129.1, 129.2, 129.9 (3), 130.0, 130.9, 135.3, 136.0, 139.3, 140.4, 147.7, 153.2 (2), 161.2, 166.1. MS, *m*/*z* (%): 584 (M^+ − 1, 60.25%), 570 (43%), 532 (52.03), 474 (43.45), 233 (69.90), 103 (100). Anal. calcd for $C_{29}H_{23}N_5O_5S_2$ (585.65): C, 59.48; H, 3.96; N, 11.96. Found C, 59.31; H, 3.90; N, 11.88%.

*2-((4-Oxo-3-phenyl-3,4-dihydroquinazolin-2-yl)thio)-N-(4-(N-(phenylcarbamothioyl) sulfamoyl)phenyl)acetamide (**7b**).* Yellow crystals, mp 244–246 °C, IR (ν, cm^{-1}): 3225, 3289, 3194 (3NH), 3062 (CH aromatic), 1649 (C=O). ^{1}H NMR (DMSO-d_6-D_2O) δ (ppm): 4.19 (s, 2H, CH_2), 7.43–7.59 (m, 11H, Ar–H), 7.78–7.83 (m, 3H, Ar–H), 7.90–7.92 (m, 3H, Ar–H), 8.06 (d, 1H, Ar–H, J = 8 Hz), 10.53 (br.s, 2H, 2NH, exchangeable), 11.04 (br.s, 1H, 1NH, exchangeable). ^{13}C NMR (100 MHz, DMSO-d_6) δ (ppm): 52.3, 118.9 (3), 119.9, 124.5, 126.4 (2), 127.02 (2), 129.9 (3), 130.0 (3),

130.4, 130.7 (3), 135.3, 136.2 (2), 143.9, 147.5, 157.27, 161.1, 166.2, 167.7. Anal. calcd for $C_{29}H_{23}N_5O_4S_3$ (601.7): C, 57.89; H, 3.85; N, 11.64. Found: C, 57.72; H, 3.77; N, 11.55%.

*Synthesis of N-(4-(6-amino-5-cyano-4-(4-aryl)pyridin-2-yl) phenyl)-2-((4-oxo-3-phenyl-3,4-dihydroquinazolin-2-yl)thio) acetamide (**8a–c**)*

(a) Conventional method. A mixture of the acetyl derivative **5b** (2 mmol), malononitrile (2 mmol) and the appropriate benzaldehyde derivative, namely 4-methoxy-, 4-chloro- or 4-nitrobenzaldehyde (2 mmol), and ammonium acetate (4 mmol) in absolute ethanol (20 mL) was heated under reflux for 8 h. The solid obtained upon cooling was collected and recrystallized from ethanol to produce the enaminonitrile derivatives **8a–c**, respectively.

(b) Microwave method. A mixture of the acetyl derivative **5b** (2 mmol), malononitrile (2 mmol) and the appropriate benzaldehyde derivative, namely 4-methoxy-, 4-chloro- or 4-nitrobenzaldehyde (2 mmol), in dioxane (4 mL) containing ammonium acetate (4 mmol) was added to the reaction vessel of the monomodal Emrys™ Creator microwave synthesizer and allowed to react under microwave irradiation at 200–400 W power for 2–4 min. The automatic mode stirring helped with mixing and uniformly heating the reactants. The reaction vessel was cooled to room temperature. The solid compound was collected by filtration, washed with water, and recrystallized from the ethanol mixture to afforded products **8a–c**, respectively.

*N-(4-(6-Amino-5-cyano-4-(4-methoxyphenyl)pyridin-2-yl) phenyl)-2-((4-oxo-3-phenyl-3,4-dihydroquinazolin-2-yl)thio) acetamide (**8a**).* Yellow crystals, mp 164–166 °C, IR (ν, cm^{-1}): 3318 (NH), 3062 (CH aromatic), 2836 (CH aliphatic), 2216 (CN), 1687 (C=O); ^{1}H NMR (DMSO-d_6-D_2O) δ (ppm): 3.85 (s, 3H, OCH_3), 4.13 (s, 2H, CH_2), 6.89–7.22 (m, 4H, Ar–H), 7.48 (br.s, 2H, NH_2, exchangeable), 7.50–7.74 (m, 6H, Ar–H), 7.81–7.83 (m, 4H, Ar–H), 7.93–7.95 (d, 2H, Ar–H, J = 8 Hz), 8.08–8.12 (d, 2H, Ar–H, J = 8 Hz), 10.71 (br.s, 1H, NH, exchangeable). ^{13}C NMR (100 MHz, DMSO-d_6) δ (ppm): 27.0, 55.8, 114.0 (3), 114.3, 115.1 (2), 118.7, 119.0 (2), 119.7, 112.2 (2), 126.3 (2), 126.8 (2), 130.0 (6), 130.6 (2), 131.4 (2), 136.0, 144.1 (2), 147.1 (2), 160.7, 166.4. Anal. calcd for $C_{35}H_{26}N_6O_3S$ (615.69): C, 68.84; H, 4.29; N, 13.76. Found: C, 68.66; H, 4.20; N, 13.65%.

*N-(4-(6-Amino-4-(4-chlorophenyl)-5-cyanopyridin-2-yl)phenyl)-2-((4-oxo-3-phenyl-3,4-dihydroquinazolin-2-yl)thio)acetamide (**8b**).* White crystals, mp 132–134 °C, IR (ν, cm^{-1}): 3242, 3179 (NH), 3037 (CH aromatic), 2855 (CH aliphatic), 2226 (CN), 1686, 1671 (C=O). ^{1}H NMR (DMSO-d_6-D_2O) δ (ppm): 4.12 (s, 2H, CH_2), 7.45–7.53 (m, 5H, Ar–H of phenyl ring), 7.60–7.62 (m, 2H, Ar–H), 7.72–7.75 (m, 4H, Ar–H), 7.79–7.83 (m, 1H, Ar–H), 7.93–7.97 (m, 5H, Ar–H), 8.07–8.09 (d, 1H, Ar–H, J = 8 Hz), 8.55 (br.s, 2H, NH_2, exchangeable), 10.70 (br.s, 1H, NH, exchangeable). MS, m/z, (%): 616 (M^+ + 1, 19.83%), 614 (17.20), 605 (42.65), 156 (100%). Anal. calcd for $C_{34}H_{23}ClN_6O_2S$ (615.11): C, 66.39; H, 3.77; N, 13.66. Found: C, 66.18; H, 3.61; N, 13.54%.

*N-(4-(6-Amino-4-(4-nitrophenyl)-5-cyanopyridin-2-yl)phenyl)-2-((4-oxo-3-phenyl-3,4-dihydroquinazolin-2-yl)thio)acetamide (**8c**).* Yellow crystals, mp 152–154 °C, IR (ν, cm^{-1}): 3285 (NH, NH_2), 2855 (CH aliphatic), 3037 (CH aromatic), 2226 (CN), 1686 (C=O). ^{1}H NMR (DMSO-d_6-D_2O) δ (ppm): 4.12 (s, 2H, CH_2), 7.47–7.53 (m, 5H, Ar–H of phenyl ring), 7.51–7.73 (m, 6H, Ar–H), 7.75–8.35 (m, 7H, Ar–H), 9.04 (br.s, 2H, NH_2, exchangeable), 10.71 (br.s, 1H, NH, exchangeable). ^{13}C NMR (100 MHz, DMSO-d_6) δ (ppm): 27.7, 89.7, 117.0, 118.7, 119.0, 119.7 (5), 124.1, 126.3 (2), 126.8 (2), 129.9, 130.6 (4), 130.3 (2), 132.5 (2), 135.2, 136.0, 143.4, 147.4, 157.4, 161.2, 166.6, 170.2, 166.95, 197.0. Anal. calcd for $C_{34}H_{23}N_7O_4S$ (625.66): C, 65.27; H, 3.71; N, 15.67. Found: C, 65.14; H, 3.60; N, 15.70%.

*Synthesis of chalcones, N-(4-(3-(4-aryl)acryloyl)phenyl)-2-((4-oxo-3-phenyl-3,4-dihydroquinazolin-2-yl)thio) acetamide (**9a–c**)*

(a) Conventional method. To a solution of the acetyl derivative **5b** (2 mmol) and the appropriate benzaldehyde derivatives, namely 4-methoxy-, 4-chloro- or 4-nitro-benzaldehyde (2 mmol) in ethanol (20 mL), sodium hydroxide (40%) was added under stirring. The reaction mixture was further stirred at room temperature for 8 h. The precipitated solid was collected, washed with water, dried, and recrystallized from dioxane to produce the chalcone derivatives **9a–c**, respectively.

(b) Microwave method. A mixture of **5b** (2 mmol) and the appropriate benzaldehyde derivatives, namely 4-methoxybenzaldehyde, 4-chlorobenzaldehyde or 4-nitrobenzaldehyde (2 mmol) in dioxane (3 mL) containing two drops of piperidine, were added to the reaction vessel of the monomodal Emrys™ Creator microwave synthesizer and allowed to react under microwave irradiation at 200–400 W power for (2–3) min. The automatic mode stirring helped with mixing and uniformly heating the reactants. The reaction vessel was cooled to room temperature. The solid compound was collected by filtration, washed with water, and recrystallized from dioxane to give products **9a–c**, respectively.

*N-(4-(3-(4-Methoxyphenyl)acryloyl)phenyl)-2-((4-oxo-3-phenyl-3,4-dihydroquinazolin-2-yl)thio)acetamide (**9a**).* Yellow crystals, mp 338–340 °C, IR (ν, cm^{-1}): 3266 (NH), 3037 (CH aromatic), 2836 (CH aliphatic), 1652 (C=O). ^{1}H NMR (DMSO-d_6-D_2O) δ (ppm): 3.79 (s, 3H, CH_3), 3.84 (s, 2H, CH_2) 6.88–6.92 (d, 1H, CH=C<u>H</u>, J = 18 Hz), 6.99–7.12 (m, 5H, Ar–H of phenyl ring), 7.57–7.86 (m, 6H, Ar–H + 1H, CH=C<u>H</u>), 7.89–8.26 (m, 6H, Ar–H), 9.85 (br.s, 1H, NH, exchangeable). Anal. calcd for $C_{32}H_{25}N_3O_4S$ (547.63): C, 70.18; H, 4.60; N, 7.67. Found: C, 70.02; H, 4.65; N, 7.73%.

*N-(4-(3-(4-Chlorophenyl)acryloyl)phenyl)-2-((4-oxo-3-phenyl-3,4-dihydroquinazolin-2-yl)thio)acetamide (**9b**).* Yellow crystals, mp 186–187 °C (decomp.), IR (ν, cm^{-1}): 3318 (NH), 3062 (CH aromatic), 2855 (CH aliphatic), 1677 (C=O). ^{1}H NMR (DMSO-d_6-D_2O) δ (ppm): 4.11 (s, 2H, CH_2), 7.23–7.35 (m, 2H, Ar–H), 7.43–7.60 (m, 5H, Ar–H + 2H, C<u>H</u>=C<u>H</u>), 7.69–7.82 (m, 5H, Ar–H), 7.90–7.99 (m, 3H, Ar–H), 8.08 (d, 1H, Ar–H, J = 8 Hz), 8.19 (d, 1H, Ar–H, J = 8 Hz), 10.78 (br.s, 1H, NH, exchangeable). ^{13}C NMR (100 MHz, DMSO-d_6) δ (ppm): 26.7, 116.3, 119.0, 119.2, 119.5, 126.5, 127.1 (2), 129.2 (4), 129.5 (2), 130.3, 130.6 (3), 131.4, 134.1, 134.4 (2), 134.9, 136.3, 136.6, 161.2, 167.1, 169.1, 169.7, 174.4, 184.2. MS, m/z, (%): 554 (M^+ + 2, 48), 552 (M^+, 100), 533 (89), (479, 40). Anal. calcd for $C_{31}H_{22}ClN_3O_3S$ (552.05): C, 67.45; H, 4.02; N, 7.61. Found: C, 67.28; H, 3.89; N, 7.64%.

*N-(4-(3-(4-Nitrophenyl)acryloyl)phenyl)-2-((4-oxo-3-phenyl-3,4-dihydroquinazolin-2-yl)thio)acetamide (**9c**).* Yellow crystals, mp 244–246 °C, IR (ν, cm^{-1}): 3362 (NH), 2855 (CH aliphatic), 1645 (C=O). ^{1}H-NMR (DMSO-d_6-D_2O) δ (ppm): 4.10 (s, 2H, CH_2), 6.58–6.65 (m, 2H, Ar–H of phenyl), 7.01–8.29 (m, 15H, Ar–H + 2H, CH=CH), 10.67 (br.s, 1H, NH, exchangeable). Anal. calcd for $C_{31}H_{22}N_4O_5S$ (562.60): C, 66.18; H, 3.94; N, 9.96. Found: C, 65.88; H, 3.83; N, 9.84%.

*Synthesis of 2-hydrazinyl-3-phenylquinazolin-4(3H)-one (**11**).* A mixture of quinazoline derivative **5a** (2mmol) and hydrazine hydrate (2 mmol, 80%) in *n*-butanol (20 mL) was heated under reflux for 6 h. The obtained solid after cooling the reaction mixture was collected by filtration and recrystallized from ethanol to furnish hydrazinoquinazoline **11** as colorless crystals, mp 207–209 °C, which was identical in all respects (melting point, mixed melting point, TLC, and IR) to an authentic sample prepared from refluxing a solution of quinazoline **3** and hydrazine hydrate in absolute ethanol for ~4–5 h (until all H_2S evolved).[23]

*Synthesis of dihydroquinazoline derivatives **12a–c***

(a) Conventional method. A mixture of compound **11** (2 mmol), 2-chloro-*N*-acetamide derivatives, namely methyl 4-(2-chloroacetamido)benzoate, *N*-(4-acetylphenyl)-2-chloroacetamide or 2-chloro-*N*-(4-sulfamoylphenyl)acetamide (**4a–c**) (2 mmol), and anhydrous sodium acetate (2 mmol) in dioxane (15 mL) was heated under reflux for 6 h. The obtained product after cooling was collected and recrystallized from the appropriate solvent to acquire compounds **12a–c**, respectively.

(b) Microwave method. An equimolar mixture of compound **11** and 2-chloro-*N*-acetamide derivatives, namely methyl 4-(2-chloroacetamido)benzoate, *N*-(4-acetylphenyl)-2-chloroacetamide or 2-chloro-*N*-(4-sulfamoyl-phenyl)acetamide (**4a–c**) (2 mmol) in DMF (2 mL) containing two drops of triethylamine, was added to the reaction vessel of the monomodal Emrys™ Creator microwave synthesizer and allowed to react under microwave irradiation at 200–400 W power for (2–3) min. The automatic mode stirring helped with mixing and uniformly heating the reactants. The reaction vessel was cooled to room temperature. The solid compound was collected by filtration, washed with water, and recrystallized from a suitable solvent to afford quinazoline derivatives **12a–c**.

*Methyl 4-(2-(2-(4-oxo-3-phenyl-3,4-dihydroquinazolin-2-yl) hydrazinyl)acetamido)benzoate (**12a**).* White crystals, mp >360 °C (ethanol/dioxane, 1 : 1), IR (ν, cm^{-1}): 3420, 3285 (NH), 2855 (CH aliphatic), 1690, 1663 (C=O). ^{1}H NMR (DMSO-d_6-D_2O) δ (ppm): 3.79 (s, 3H, CH_3), 4.14 (s, 2H, CH_2), 4.67 (br.s, 1H, 1NH, exchangeable), 7.42–7.47 (m, 2H, Ar–H + 1H, NH, exchangeable), 7.51–7.58 (m, 3H, Ar–H), 7.76–7.79 (m, 5H, Ar–H), 7.87–7.89 (m, 2H, Ar–H), 8.04 (d, 1H, Ar–H, J = 8 Hz), 11.20 (br.s, 1H, NH, exchangeable). ^{13}C NMR (100 MHz, DMSO-d_6) δ (ppm): 23.5, 40.3, 117.12, 118.3, 123.9 (2), 127.5 (2), 128.1 (2), 129.2 (4), 129.5 (4), 135.4 (2), 140.5, 142.7, 160.9, 176.3. Anal. calcd for $C_{24}H_{21}N_5O_4$ (443.46): C, 65.00; H, 4.77; N, 15.79. Found: C, 64.78; H, 4.69; N, 15.66%.

*N-(4-Acetylphenyl)-2-(2-(4-oxo-3-phenyl-3,4-dihydroquinazolin-2-yl)hydrazinyl)acetamide (**12b**).* Beige crystals, mp 183–185 °C (decomp.) (ethanol), IR (ν, cm^{-1}): 3336 (NH), 3056 (CH aromatic), 1678 (C=O). ^{1}H NMR (DMSO-d_6-D_2O) δ (ppm): 2.55 (s, 3H, $COCH_3$), 3.44 (s, 2H, CH_2), 4.32 (br.s, 1H, NH, exchangeable), 7.14–7.32 (m, 2H, Ar–H), 7.36–7.51 (m, 5H, Ar–H + 1H, NH exchangeable), 7.56–7.77 (m, 3H, Ar–H), 7.81–7.99 (m, 3H, Ar–H), 10.56 (br.s, 1H, NH, exchangeable). Anal. calcd for $C_{24}H_{21}N_5O_3$ (427.46): C, 67.44; H, 4.95; N, 16.38. Found: C, 67.31; H, 4.86; N, 16.40%.

*2-(2-(4-Oxo-3-phenyl-3,4-dihydroquinazolin-2-yl)hydrazinyl)-N-(4-sulfamoylphenyl)-acetamide (**12c**).* Beige crystals, mp 274–276 °C (ethanol/dioxane, 1 : 1), IR (ν, cm^{-1}): 3317, 3217 (NH, NH_2), 3068 (CH aromatic), 1672 (C=O). ^{1}H NMR (DMSO-d_6-D_2O) δ (ppm): 4.13 (s, 2H, CH_2), 7.27 (br.s, 2H, NH_2, exchangeable), 7.31 (br.s, 1H, NH, exchangeable), 7.45–7.53 (m, 5H, Ar–H of phenyl ring), 7.60–7.62 (m, 2H, Ar–H + 1H, NH, exchangeable), 7.78–7.84 (m, 5H, Ar–H), 8.09 (d, 1H, Ar–H, J = 8 Hz), 10.71 (br.s, 1H, NH, exchangeable). ^{13}C NMR (100 MHz, DMSO-d_6) δ (ppm): 37.9, 119.0 (2), 120.0, 126.1, 126.3, 126.5, 127.2 (3), 129.8 (2), 130.2, 130.5, 135.3, 136.0, 138.9, 142.2, 147.7, 157.0, 160.7, 166.7. Anal. calcd for $C_{22}H_{20}N_6O_4S$ (464.50): C, 56.89; H, 4.34; N, 18.09. Found: C, 56.76; H, 4.26; N, 17.98%.

*Condensation of **11** with different aromatic aldehydes*

(a) Conventional method. A solution of hydrazine derivative **11** (2 mmol) and the appropriate aromatic aldehyde, namely 2-hydroxybenzaldehyde, 4-hydroxybenzaldehyde, 2-methoxybenzaldeyde, and 4-nitrobenzaldehyde (2 mmol) in glacial acetic acid (10 mL), was heated under reflux for 30 min. The precipitated solid while heating was collected and recrystallized from dioxane to afford the corresponding hydrazone derivatives **13a–d**, respectively.

(b) Microwave method. A mixture of hydrazine derivative **11** (2 mmol) and the appropriate aromatic aldehyde, namely 2-hydroxybenzaldehyde, 4-hydroxybenzaldehyde, 2-methoxybenzaldeyde, or 4-nitrobenzaldehyde (2 mmol) in glacial acetic acid (3 mL), was added to the reaction vessel of the monomodal Emrys™ Creator microwave synthesizer and allowed to react under microwave irradiation at 200–400 W power for 1–2 min. The automatic mode stirring helped with mixing and uniformly heating the reactants. The reaction vessel was cooled to room temperature. The solid compound was collected by filtration, washed with water, and recrystallized from dioxane to achieve products **13a–d**, respectively.

*2-(2-(2-Hydroxybenzylidene)hydrazinyl)-3-phenylquinazolin-4(3H)-one (**13a**).* Yellow crystals, mp 341–343 °C, IR (ν, cm^{-1}): 3248, 3221 (NH), 3036 (CH aromatic), 2872 (CH aliphatic), 1662 (C=O). ^{1}H NMR (DMSO-d_6-D_2O) δ (ppm): 6.83–7.90 (m, 2H, Ar–H), 7.15–7.34 (m, 3H, Ar–H), 7.49–7.56 (m, 4H, Ar–H), 7.64–7.67 (m, 2H, Ar–H), 7.82 (d, 1H, Ar–H, J = 8 Hz), 7.91–7.97 (m, 1H, Ar–H), 8.22 (s, 1H, N=CH), 10.25 (br.s, 1H, NH, exchangeable), 10.67 (br.s, 1H, OH, exchangeable). ^{13}C NMR (100 MHz, DMSO-d_6) δ (ppm): 114.8, 116.2, 116.4, 119.6, 120.7, 122.3, 124.9, 127.8, 128.3, 129.3 (2), 129.4, 129.7, 131.46, 135.5, 137.0, 140.3, 150.7, 153.7, 157.2, 161.0. MS, *m*/*z*, (%): 357 (M^+ + 1, 44%), 356 (M^+, 100%), 355, (76). Anal. calcd for $C_{21}H_{16}N_4O_2$ (356.39): C, 70.77; H, 4.53; N, 15.72. Found: C, 70.45; H, 4.42; N, 15.61%.

*2-(2-(4-Hydroxybenzylidene)hydrazinyl)-3-phenylquinazolin-4(3H)-one (**13b**).* White crystals, mp 320–322 °C, IR (ν, cm^{-1}):

3322 (NH&OH), 3059 (CH aromatic), 2925 (CH aliphatic), 1700 (C=O), 1620 (C=N). ^{1}H NMR (DMSO-d_6-D_2O) δ (ppm): 6.79 (d, 2H, Ar–H C_6H_4OH, $J = 8.4$ Hz), 7.13–7.17 (m, 1H, Ar–H of phenyl group), 7.32 (d, 2H, Ar–H, C_6H_4OH, $J = 8.4$ Hz), 7.40–7.76 (m, 7H, Ar–H), 7.90 (d, 1H, Ar–H, $J = 8.4$ Hz), 7.95 (s, 1H, N=CH), 9.83 (br.s, 1H, NH, exchangeable), 10.47 (br.s, 1H, OH, exchangeable). Anal. calcd for $C_{21}H_{16}N_4O_2$ (356.39): C, 70.77; H, 4.53; N, 15.72; Found: C, 70.59; H, 4.60; N, 15.60%.

*2-(2-(2-Methoxybenzylidene)hydrazinyl)-3-phenylquinazolin-4(3H)-one (**13c**).* White crystals, mp 274–276 °C, IR (ν, cm^{-1}): 3339 (NH), 3054 (CH aromatic), 2834 (CH aliphatic), 1686 (C=O), 1613 (C=N). ^{1}H NMR (DMSO-d_6-D_2O) δ (ppm): 3.79 (s, 3H, OCH_3), 7.00–7.05 (m, 2H, Ar–H), 7.16–7.18 (m, 1H, Ar–H), 7.32–7.52 (m, 4H, Ar–H), 7.68 (m, 2H, Ar–H), 7.91 (d, 2H, Ar–H, $J = 8$ Hz), 8.28 (s, 1H, N=CH), 8.29 (d, 2H, Ar–H, $J = 8$ Hz), 10.59 (br.s, 1H, NH, exchangeable). Anal. calcd for $C_{22}H_{18}N_4O_2$ (370.41): C, 71.34; H, 4.90; N, 15.13; Found: C, 71.21; H, 4.82; N, 15.06%.

*2-(2-(4-Nitrobenzylidene)hydrazinyl)-3-phenylquinazolin-4(3H)-one (**13d**).* Orange crystals, mp 330–332 °C, IR (ν, cm^{-1}): 3202 (NH), 3061 (CH aromatic), 2925 (CH aliphatic), 1665 (C=O), 1620 (C=N). ^{1}H NMR (DMSO-d_6-D_2O) δ (ppm): 7.20–7.24 (m, 1H, Ar–H), 7.36 (d, 2H, Ar–H, C_6H_4–NO_2, $J = 8$ Hz), 7.41–7.53 (m, 5H, Ar–H), 7.70–7.76 (m, 2H, Ar–H), 7.95 (d, 1H, Ar–H, $J = 8$ Hz), 8.18–8.27 (m, 2H, Ar–H + 1H, N=CH), 10.59 (br.s, 1H, NH, exchangeable). Anal. calcd for $C_{21}H_{15}N_5O_3$ (385.38): C, 65.45; H, 3.92; N, 18.17. Found: C, 65.22; H, 3.83; N, 18.10%.

5.2. Bioassay

5.2.1. PARP inhibition assay

Assay procedure. PARP-1 enzyme inhibition activity was measured using a colorimetric 96-well PARP-1 assay kit (catalog no. 80580) (BPS Bioscience), according to the manufacturer's protocol. Briefly, the histone mixture was diluted 1 : 5 with 1× PBS, and 50 μL of histone solution was added to each well and incubated at 4 °C overnight. The plate was washed three times using 200 μL PBST buffer (1× PBS containing 0.05% Tween-20) per well. Liquid was removed from the wells by tapping the strip wells on clean paper towels. To each well, 200 μL of blocking buffer was added, followed by 60–90 min incubation at room temperature. Then, 25 μL of PARP master mixture (consisting of 2.5 μL 10× PARP buffer + 2.5 μL 10× PARP assay mixture + 5 μL activated DNA + 15 μL distilled water) was added to each well. **Olaparib** was used as a positive control. 5 μL of inhibitor solution was added to each well labeled as "Test Inhibitor". For the "Positive Control" and "Blank", 5 μL of the same solution without inhibitor was added. 1× PARP buffer was prepared by adding 1 part of 10× PARP buffer to 9 parts H_2O (v/v), and 20 μL of 1× PARP buffer was added to the wells designated as "Blank". The amount of PARP-1 required for the assay was then calculated. The reaction was initiated by adding 20 μL of diluted PARP-1 enzyme to the wells designated "Positive Control" and "Test Inhibitor Control". The strip wells were incubated at room temperature for 1 hour. The strip wells were then washed three times with 200 μL of PBST buffer. Then, 50 μL of 50 times diluted Streptavidin-HRP with blocking buffer was added to each well, and the strips were further incubated at room temperature for 30 min. After washing the wells three times with 200 μL of PBST buffer, HRP colorimetric substrate was added to each well and the plate was incubated at room temperature until a blue color was developed in the positive control well. Then, the reaction was quenched with 100 mL per well of 2 M sulfuric acid. Carrier solvent (DMSO 5%, v/v) was used as a negative control. All compounds including **Olaparib** were tested at 5 concentrations (100, 10, 1, 0.1, and 0.01 μM). The optical density (OD) of each well was measured spectrophotometrically at 450 nm with an ELISA microplate reader (ChroMate-4300, FL, USA). The IC_{50} values were calculated according to the equation for Boltzmann sigmoidal concentration–response curves using the nonlinear regression fitting model (GraphPad Prism Version 8). All assays were performed in triplicate in 3 repeated experiments. The obtained data are presented means ± standard error of the means from 3 independent repeats ($n = 3$).

5.3. *In silico* studies

5.3.1. Docking methodology. A molecular modeling simulation study was performed through docking of the target compounds in the binding site of the PARP-1 enzyme using the C-Docker protocol in Discovery Studio 2.5 Software. The X-ray crystal structure of **Olaparib** in complex with PARP-1 was downloaded from http://www.rscb.org/pdb (PDB ID: 5DS3) in PDB format. Computational docking is an automated computer based algorithm designed to estimate two main terms. The first is to determine the suitable position and the orientation of a certain test set molecule's pose inside the binding site in comparison to that of the X-ray crystallographic enzyme–substrate complex. The second term is the calculation of the estimated protein ligand interaction energy, which is known as docking scoring.

5.3.2. QSAR study. The QSAR study was performed using Discovery Studio 2.5 Software. The training set was composed of **18** compounds, the **17** synthesized compounds (**5a**, **5b**, **5c**, **6a**, **6b**, **8a**, **8b**, **8c**, **9a**, **9b**, **9c**, **12a**, **12b**, **12c**, **13a**, **13c** and **13d**) and **Olaparib**. The internal validation for the QSAR model used employed leave one-out cross-validation, external validation using a test set composed of three of the synthesized compounds (**7a**, **7b** and **13b**), and residuals between the predicted and experimental activity of the training set and test set. The "calculate molecular properties" module was used in calculating the 2D molecular properties and the energies of the highest occupied and lowest unoccupied molecular orbitals (HOMO and LUMO)[40,41] of each of the training set compounds were determined. 2D descriptors included AlogP, fingerprints, surface area and volume, molecular properties such as molecular formula, molecular composition, molecular weight, molecular solubility and pK_a, molecular property counts such as HBA_Count, HBD_Count, Num_Aromatic rings and Num_Rotatable bonds, and topological descriptors.[42]

The genetic function approximation model was employed to search for optimal QSAR models that combine high quality

binding pharmacophores with other molecular descriptors and are capable of correlating bioactivity variation across the used training set collection. The trials were held while changing the independent properties until the best model with the least variables was obtained. The QSAR model was validated employing leave one-out cross-validation, r^2 (squared correlation coefficient value), and external validation using compounds **7a**, **7b** and **13b**, as well as residuals between the predicted and experimental activity of the training and test set.

Conflicts of interest

The authors declare no conflict of interest, financial or otherwise.

Acknowledgements

The authors would like to extend their sincere appreciation to Dr Ahmed Esmat from the Department of Pharmacology, Faculty of Pharmacy, ASU for his help in revising the biology. We also thank the center for drug discovery and development research at ASU for performing NMR spectral analysis. In addition, we gratefully acknowledge the scientific research team of VASERA CO. Giza, Egypt, for providing laboratory facilities for biological activity.

References

1 M. Rouleau, A. Patel, M. J. Hendzel, S. H. Kaufmann and G. G. Poirier, *Nat. Rev. Canc.*, 2010, **10**, 293–301.
2 E. A. Comen and M. Robson. *Oncology*, Williston Park, N.Y., 2010, vol. 24, pp. 55–62.
3 F. J. Bock and P. Chang, New directions in poly(ADP-ribose) polymerase biology, *FEBS J.*, 2016, **83**, 4017–4031.
4 H. E. Bryant, N. Schultz, H. D. Thomas, K. M. Parker, D. Flower, E. Lopez, S. Kyle, M. Meuth, N. J. Curtin and T. Helleday, *Nature*, 2005, **434**, 913–917.
5 T. A. Yap, S. K. Sandhu, C. P. Carden and J. S. de Bono, *Ca-Cancer J. Clin.*, 2011, **61**, 31–49.
6 R. Scully, *Breast Cancer Res.*, 2000, **2**, 324–330.
7 N. Curtin, PARP inhibitors for anticancer therapy, *Biochem. Soc. Trans.*, 2014, **42**, 82–88.
8 Y. Nonomiya, K. Noguchi, K. Katayama and Y. Sugimoto, *Biochem. Biophys. Res. Commun.*, 2019, **510**, 501–507.
9 B. Sahu, A. Narota and A. S. Naura, *Eur. J. Pharmacol.*, 2020, **87715**, 173091.
10 M. M. AlHilli, M. A. Becker and P. Haluska, *J. Gynecol. Oncol.*, 2016, **143**, 379–388.
11 A. C. Houts, T. Olufade, R. Shenolikar, M. S. Walker and L. S. Schwartzberg, *Cancer Treat. Res. Commun.*, 2019, **19**, 100121.
12 L. Lehtio, A. S. Jemth, R. Collins, O. Loseva, A. Johansson, N. Markova, M. Hammarstrom, A. Flores, L. Holmberg-Schiavone, J. Weigelt, T. Helleday, H. Schuler and T. Karlberg, *J. Med. Chem.*, 2009, **52**, 3108–3111.
13 Y. Q. Wang, P. Y. Wang, Y. T. Wang, G. F. Yang, A. Zhang and Z. H. Miao, *J. Med. Chem.*, 2016, **59**, 9575–9598.
14 P. G. Jain and B. D. Patel, *Eur. J. Med. Chem.*, 2019, **165**, 198–215.
15 X. Song, X. Han, F. Yu, X. Zhang, L. Chen and C. Lv, *Theranostics*, 2018, **8**(8), 2217–2228.
16 I. A. Shagufta, *RSC Med. Chem.*, 2017, **8**, 871.
17 J. Zhou, M. Ji, H. Yao, R. Cao, H. Zhao, X. Wang, X. Chen and B. Xu, *Org. Biomol. Chem.*, 2018, **16**, 3189.
18 H. Yao, M. Ji, Z. Zhu, J. Zhou, R. Cao, X. Chen and B. Xu, *Bioorg. Med. Chem.*, 2015, **23**, 681–693.
19 I. H. Eissa, A. M. El-Naggar and M. A. El-Hashash, *Bioorg. Chem.*, 2016, **67**, 43–56.
20 S. K. Ramadan and H. A. Sallam, *J. Heterocycl. Chem.*, 2018, **55**, 1942–1954.
21 (*a*) H. Yan, X.-Q. Xiao, R. C. Hider and Y. Ma, *Front. Chem.*, 2019, **7**, 584; (*b*) K. A. M. Abouzid, G. H. Al-Ansary and A. M. El-Naggar, *Eur. J. Med. Chem.*, 2017, **134**, 357–365.
22 (*a*) M. Haghighat, F. Shirini and M. Golshekan, *J. Mol. Struct.*, 2018, **1171**, 168–178; (*b*) A. M. El-Naggar, A. K. Khalil, H. M. Zeidan and W. M. El-Sayed, *Anti-Cancer Agents Med. Chem.*, 2017, **17**, 1644–1651.
23 (*a*) A. M. Alafeefy, M. Ceruso, A. S. Al-Tamimi, S. D. Prete, C. Capasso and C. T. Supuran, *Bioorg. Med. Chem.*, 2014, **22**(19), 5133–5140; (*b*) S. K. Pandey, A. Singh and A. Singh, *Eur. J. Med. Chem.*, 2009, **44**, 1188–1197.
24 T. S. Straub, *Tetrahedron Lett.*, 1995, **36**, 663–664.
25 S. Sandler and W. Karo, in *Organic Functional Group Preparations*, 1972, vol. 3, p. 372.
26 E. D. Bergman, L. Ginsibm and R. Pappo, *Org. React.*, 1959, **10**, 179.
27 J. F. Ballesteros, M. J. Sanz, A. Ubeda, M. A. Miranda, S. Iborra, M. Paya and M. Alcaraz, *J. Med. Chem.*, 1995, **38**, 2794–2797.
28 M. L. Go, X. Wu and X. L. Liu, *Curr. Med. Chem.*, 2005, **12**, 483–499.
29 V. K. Mukerjee, A. K. Prased, A. G. Raj, M. E. Brakhe, C. E. Olsen, S. C. Jain and V. S. Parmar, *Bioorg. Med. Chem.*, 2001, **9**, 337–345.
30 U. M. Liu, P. Wilairat, S. L. Croft, A. L. Tan and M. Go, *Bioorg. Med. Chem.*, 2003, **11**, 2729–2738.
31 P. M. Sivakumar, S. K. GeethaBabu and D. Mukesh, *Chem. Pharm. Bull.*, 2007, **55**, 44.
32 N. Tiwari, B. Dwivedi, K. F. Nizamuddin, Y. Nakanshi and K. H. Lee, *Bioorg. Med. Chem.*, 2000, **10**, 699–701.
33 S. Ducki, R. Forrest, J. A. Hadfield, A. Kendall, N. J. Lawrence, A. T. Mc-Gown and D. Rennison, *Bioorg. Med. Chem.*, 1998, **8**, 1051.
34 J. Wang and M. J. Lenardo, *J. Cell Sci.*, 2000, **113**, 753–757.
35 J. M. Brown and B. G. Wouters, *Cancer Res.*, 1999, **59**, 1391–1399.
36 (*a*) Y. Huang, F. Yu, J. Wang and L. Chen, *Anal. Chem.*, 2016, **88**(7), 4122–4129; (*b*) K. K.-W. Lo, T. K.-M. Lee, J. S.-Y. Lau, W.-L. Poon and S.-H. Cheng, *Inorg. Chem.*, 2008, **47**, 200–208; (*c*) W. Zhang, Y. Wang, X. Sun, W. Wang and L. Chen, *Nanoscale*, 2014, **6**, 14514–14522.

37 J. L. Faulon and A. Bender, *Handbook of Chemoinformatics Algorithms*, CRC Press, 2010.
38 R. F. George, N. S. M. Ismail, J. Stawinski and A. S. Girgis, *Eur. J. Med. Chem.*, 2013, **68**, 339–351.
39 A. S. Girgis, J. Stawinski, N. S. M. Ismail and H. Farag, *Eur. J. Med. Chem.*, 2012, **47**, 312–322.
40 L. B. Kier and L. H. Hall, in *Molecular Connectivity in Structure-Activity Analysis, Chemometrics Series*, ed. D. D. Bawden, Research Studies Press Ltd, New York, 1985, vol. 9.
41 C. J. F. Bottcher, *Theory of Electric Polarization*, Elsevier Press: Amsterdam, 1973.
42 D. T. Stanton and P. C. Jurs, *Anal. Chem.*, 1990, **62**, 2323–2329.

